ISSN 1028-8546

Volume XXI, Number 1
Section: En
April, 2015

Azerbaijan Journal of Physics

Fizika

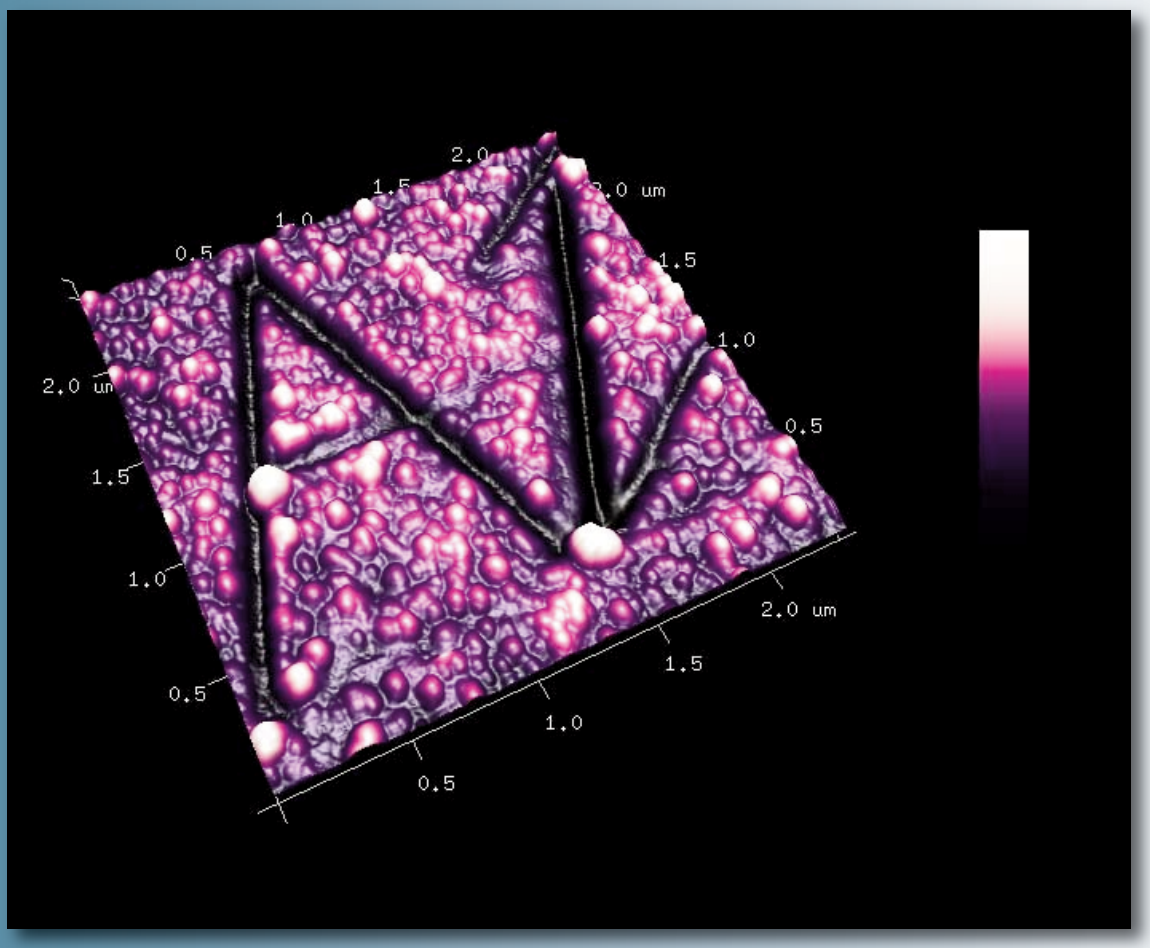

www.physics.gov.az

G.M. Abdullayev Institute of Physics
Azerbaijan National Academy of Sciences
Department of Physical, Mathematical and Technical Sciences

Published from 1995
Ministry of Press and Information
of Azerbaijan Republic,
Registration number 402, 16.04.1997

ISSN 1028-8546
vol. XXI, Number 01, 2015
Series: En

Azerbaijan Journal of Physics

FIZIKA

G.M.Abdullayev Institute of Physics
Azerbaijan National Academy of Sciences
Department of Physical, Mathematical and Technical Sciences

PUBLISHING OFFICE

131 H.Javid ave, AZ-1143, Baku
ANAS, G.M.Abdullayev Institute of Physics

Tel.: (99412) 439-51-63, 439-32-23
Fax: (99412) 447-04-56
E-mail: jophphysics@gmail.com
Internet: www.physics.gov.az

It is authorized for printing:

Published at "**SƏRQ-QƏRB**"
17 Ashug Alessger str., Baku
Typographer : Aziz Gulaliyev

Sent for printing on: __.__. 201_
Printing approved on: __.__. 201_
Physical binding:_____
Number of copies:_____200
Order:_____

LIGHT TRANSFORMATION OF DIFFERENT LENGTH WAVES IN NANO-CRYSTALS OF ALKALINE-EARTH COMPOUNDS OF $CaGa_2S_4$ TYPE

A.M. PASHAYEV[a], B.G. TAGIEV[a,b], O.B. TAGIEV[b,c], R.A. ABDULHEYOV[a] , F.A. KAZIMOVA[b]

[a]National Academy of Aviation, Bina, 25th km, AZ-1045, Baku, Azerbaijan
[b]Institute of Physics Academy of Sciences of Azerbaijan, H.Javid ave. 33, AZ-1143 Baku
[c]Branch of Moscow State University in Baku, F.Agayev str 9., AZ-1141, Baku, Azerbaijan
e-mail: oktay@physics.ab.az

The given article is dedicated to investigation results of photoluminescence (PL) in $CaGa_2S_4$: Eu nanocrystals excitated by ultraviolet (UV), emission of different wavelengths. $CaGa_2S_4$ compound is prepared in the process of solid-state chemical reaction between CaS и Ga_2S_3 at temperature about 1150° C. The activation of rare earth elements (REE) - synthesized compounds is carried out during solid-state reaction. According to S.I.Vavilov law, it is shown that PL energy efficiency in interval 300÷480nm linearly increases when the excitation light wavelength increases. The maxima at 420, 440, 460, 485nm of wavelengths are revealed on excitation spectrum of $CaGa_2S_4:Eu^{2+}$ nanocrystals. The energy of given excitation light wavelengths effectively transforms into visible light energy.

Keywords: photoluminescence, nanocrystals, rare earth elements, compounds.
PACS: 76.30, 78.55

INTRODUCTION

The compounds of $CaGa_2S_4$ type relate to vast class of high-ohmic ($10^6 \div 10^9$Om·m) and wide bandgap semiconductors (4,0÷4,5eV) having general formula II-III_3-VI_4, where II are Pb, Eu,Yb,Ca,Sr,Ba bevalent cations; III are Ga,In, Al trivalent cations; VI are S,Se,O,Te chalcogens.

Rare-earth elements (REE) in these materials make efficient emission centers [1-4].

The triple compounds of $CaGa_2S_4$:REE type are perspective materials to transformate of electric field energy, ultraviolet (UV), infrared (IR) [1-4] and X-ray emissions and also α, γ particle energies into visible light energy. Under influence of these factors, the undoped compounds of $CaGa_2S_4$ type have the weak structureless emission due to structural defects.

Nowadays the investigation connected with transformation of energy different types into visible light in nanocrystalline semiconductors, in particular, in wide bandgap nano-crystals from compound of II-III_3-VI_4 group, the striking representative of which is $CaGa_2S_4$:REE, is of great interest for revealing of physical mechanism, technology and practical application.

The given article is dedicated to investigation results of photoluminescence (PL) in $CaGa_2S_4$: Eu nanocrystals excitated by UV emission of different wavelengths.

THE SYNTHESIS OF $CaGa_2S_4$ COMPOUND AND SAMPLE PREPARATION FOR PL INVESTIGATION

$CaGa_2S_4$ compound is prepared in the process of solid-state chemical reaction between CaS и Ga_2S_3 at temperature about 1150° C. We use the two methods of $CaGa_2S_4$ synthesis: 1) CaS and Ga_2S_3 compounds are in evacuated quartz ampolule (10^{-4} millimeter of mercury), the mixture temperature increases up to 1000°C and the reaction continues during 5 hours.; 2) the solid-state reaction between CaS and Ga_2S_3 continues during 4 hours in graphitized quartz crucible under the activated carbon layer at temperature 1000°C. The activation of REE-synthesized compounds is carried out during solid-state reaction.

The synthesized compounds in agathic mortar are disintegrated; the obtained powders have the dimensions 5-10μm. Further, these powders are put into ball mill to desintegrate up to 10-100nm.

The luminescent material nano-particles of $CaGa_2S_4$:REE are investigated in atomic force microscope (AFM). As it is known the atomic force microscopy is the one of the progressive study methods of nanodimensional materials. Nanocrystals are prerared on surface of polished quartz glass by hand molding method.

AFM scanning from big squares (60x60μm^2) up to small (500x500nm^2) ones with the aim to choice nanodimensional surface consisted of $CaGa_2S_4$:REE nanoparticles is carried out several times in spite of the fact that surface has the smooth molded surface at visual inspection.

The scanning is carried out at room temperature under conditions *ex situ* at following parameters: the scanning speed is 3μm/sec, operating scanning area is 527x527nm^2, the scanning pitch is 4nm, the resolution is 128 points,the feedback amplification is 3, the operating point is 0,6. The scanning surface in 2D format is shown on fig.1. From figures 1 and 2 it is seen that obtained surface has the certain order both on X, Y and Z axes. The order is more visually seen on profillograms of different cross sections of given surface shown on fig.3.

From fig.3 one can conclude that the surface consist of molded or bound together clusters $CaGa_2S_4$:REE with height dimensions not more ~20nm on the average, the lateral dimensions of which are commensurable with height ones ~20nm. From this it is followed that $CaGa_2S_4$:REE nanoparticles obtained in ball mill have the dimension ~20nm independently on direction.

Histogram shows that chosen surface irregularity have mainly the dimensions from 20nm up to 55nm in terms of nambers (fig.4).

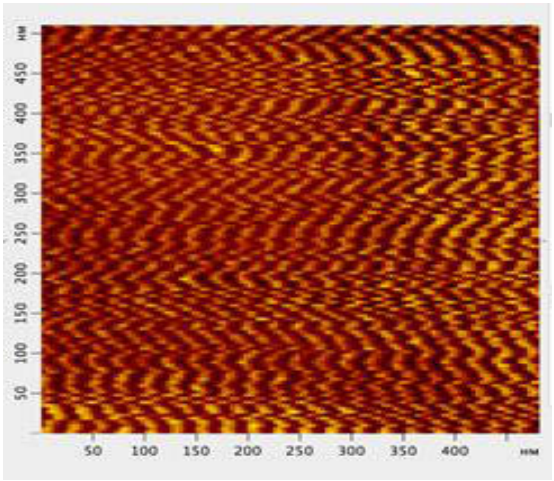

Fig.1. 2D format AFM of $CaGa_2S_4$ nano-crystal surface after scanning area decrease.

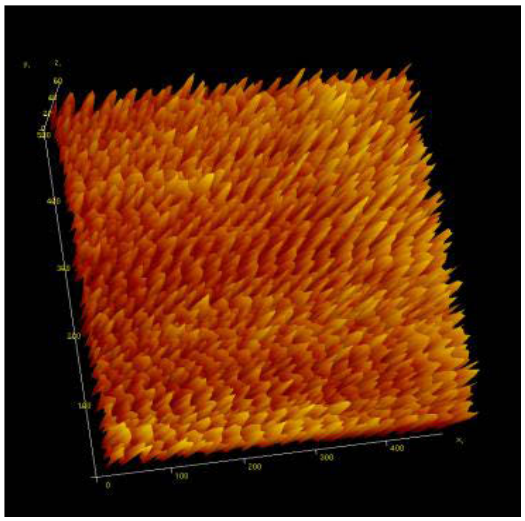

Fig.2. 3D format AFM of $CaGa_2S_4$ nano-crystal surface of the given surface on fig.1.

MEASUREMENT RESULTS AND THEIR DISCUSSION.

Experimental results show that the $CaGa_2S_4:Eu^{2+}$ poly crystal disintegration leads to weakening of luminescent properties (luminance decrease, loss of luminescent ability, luminescence damping, luminescence color change and others). However, this fact doesn't influence on use of this compound at preparation of light sorces and light emitting diode.

The problem of optical property variations (including luminescent one) of crystal phosphors at their disintegration is analyzed in [5-7]. In these works it is shown that investigation of obtained nano-dimensional $CaGa_2S_4:Eu^{2+}$ property crystals leads to the conclusion on luminescence molecular nature and luminance decrease is defined by change of excitation light dispersion. The excitation spectrum representing itself the dependence of luminescence intensity on wavelength or frequency of excitation light takes the important place among spectral characteristics [8,9,13,14].

When the luminescence presents itself the pure intracenter process, emission absorbed by main lattice can be non-active one. In our case $CaGa_2S_4:Eu^{2+}$ has the weak structureless luminescence without activator. By excitation spectra one can study the transformation process of light quantum absorbed energy in luminescent emission one [8,13,14].

The excitation and emission spectra of polycrystals (dimensions 10÷100nm) are investigated on spectrofluorimeter "Fluorat-02-Panorama". This spectrofluorimeter allows us to exitate the photolumiunescence (PL) by different wavelengths in region 200÷690nm. The carried out measurements of PL spectra of nanodimensional powder samples at different excitation light wavelengths gives the significant information on PL energy efficiency and luminescence spectrum form.

The excitation spectrum of $CaGa_2S_4:Eu^{2+}$ nanocrystals is presented on fig.5. It is seen that maxima at 420, 440, 460 and 485nm appear in excitation spectrum. The excitation spectra have the wavelength region 360÷520nm. As it is seen from fig.5, PL intensity decreases at 490nm.

$CaGa_2S_4:Eu^{2+}$ PL spectra at different wavelengths of excitation light are shown on fig.6. From this figure one can make the following conclusions: 1) PL spectrum form doesn't depend on excitation light wavelength; 2) PL intensity maxima increase when excitation light wavelengths decrease. The analysis of investigated PL spectra presented in fig.6, shows that Stokes losses $\Delta E = E_{exc} - E_L$ decrease from 0,54 up to 0,23eV (where E_{exc} is excitation light energy, E_L is energy corresponding to PL spectrum maxima on fig.6). This shows the more wavelength λ_{exc} of excitation light the less energy losses at light transformation in effective luminophors which are $CaGa_2S_4:Eu^{2+}$ compounds. It should be noted that excitation light wavelength doesn't overlao with emission wavelength of $CaGa_2S_4$ compound. On the base of data presented in fig.6 one can conclude that PL maxima positions almost don't depend on excitation light wavelength and they correspond to $5d4f \rightarrow {}^8S_{7/2}$ electron transitions of (Eu^{2+}) europium ions.

Note that S.I.Vavilov firstly payed attention on independence of PL spectrum form on excitation light different wavelengths 90 years ago [11,12]. He introduced the perceptions of energy and quantum efficiencies for luminescence characteristics [11,12]. These parameters are analysed by many authors (see for example, [10,14,16,17]).

S.I.Vavilow shows that PL energy efficiency in Stokes region increases proprtionally to excitation light wavelength (λ_{exc}) and rapidly decreases in anti-Stokes one up to zero at further λ_{exc} increase.

The ratio of energy emitted at PL to absorbed excitation light energy is called by PL energy efficiency (B_e).

$$B_e = \frac{h\nu_{em}}{h\nu_{exc}} B_k = \frac{\lambda_{exc}}{\lambda_{em}} B_k \qquad (1)$$

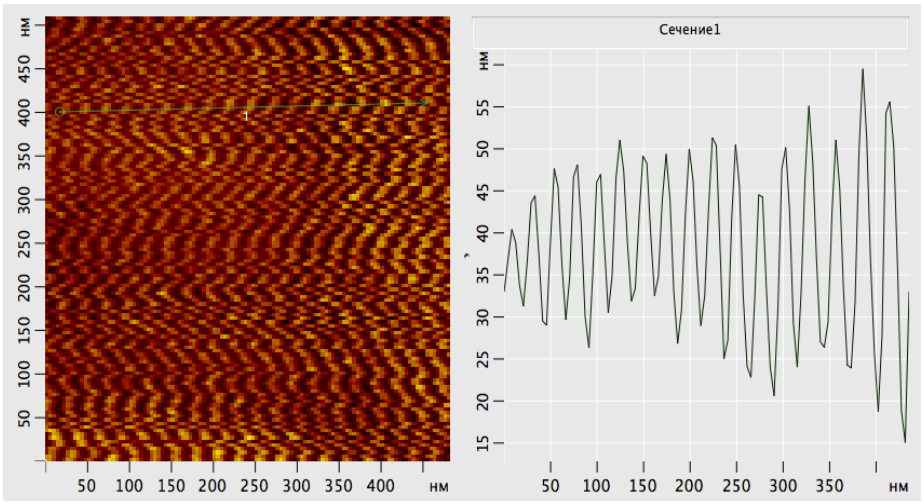

a)

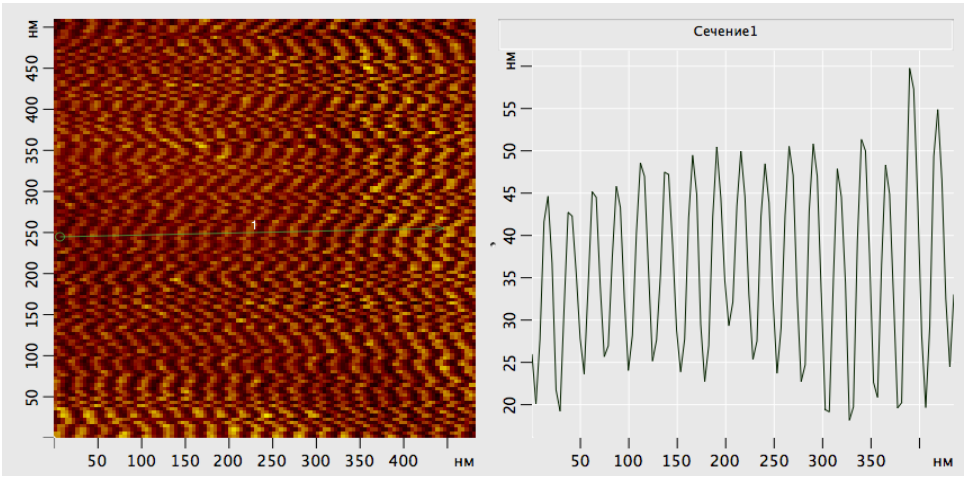

b)

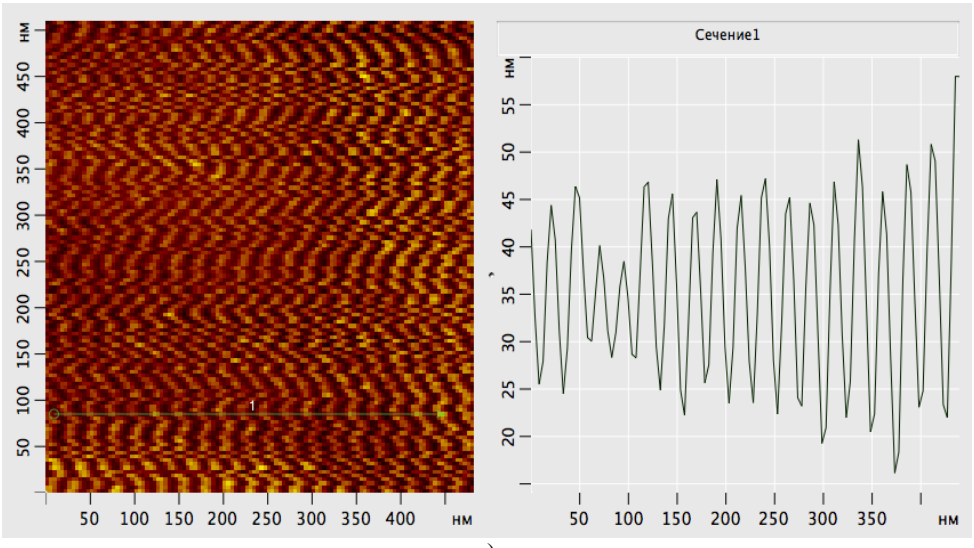

c)

Fig.3. The surface progilograms on different sections (- a);-b) and-c) from AFM sample on fig.1.

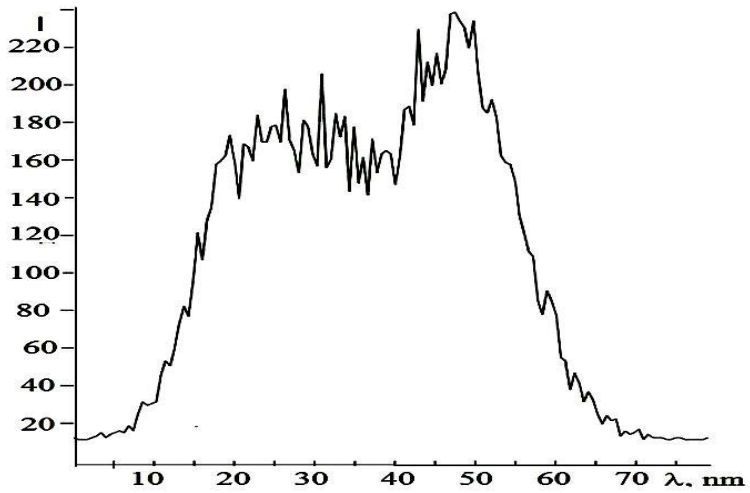

Fig.4. The surface hystograms 527x527nm^2 from fig.1.

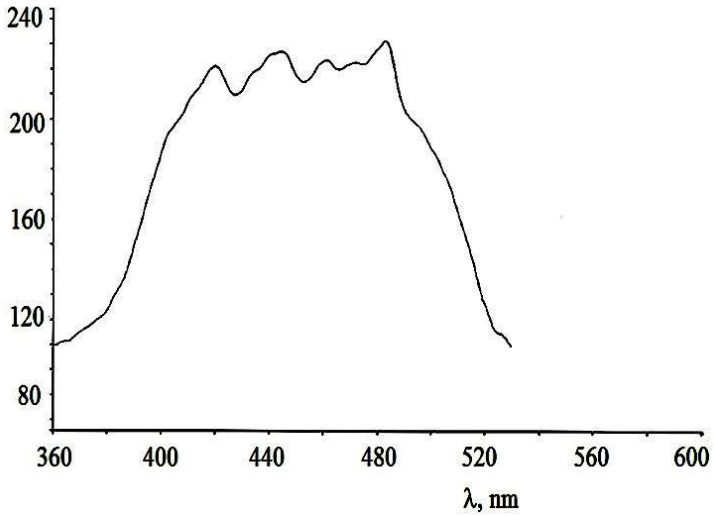

Fig.5. Excitation spectrum $CaGa_2S_4$ Eu^{+2} at T=300K.

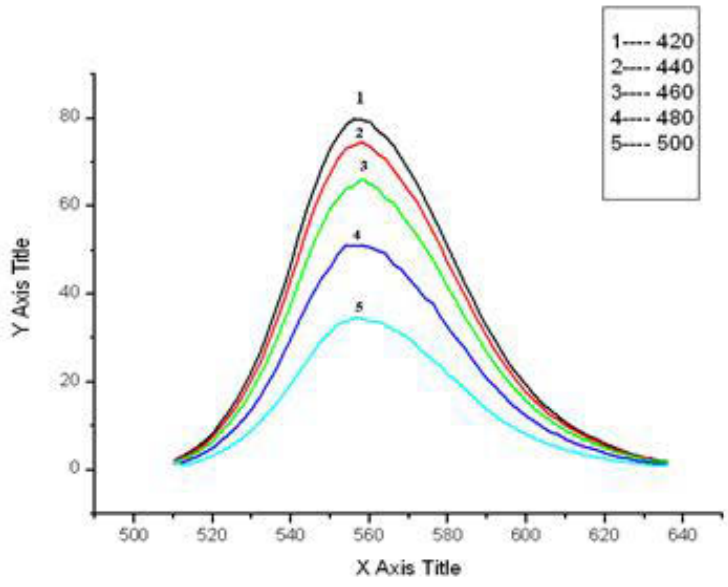

Fig.6. Photoluminescence of $CaGa_2S_4$ Eu^{+2} nanocrystals at different excitation light wave lengths. T=300 K.

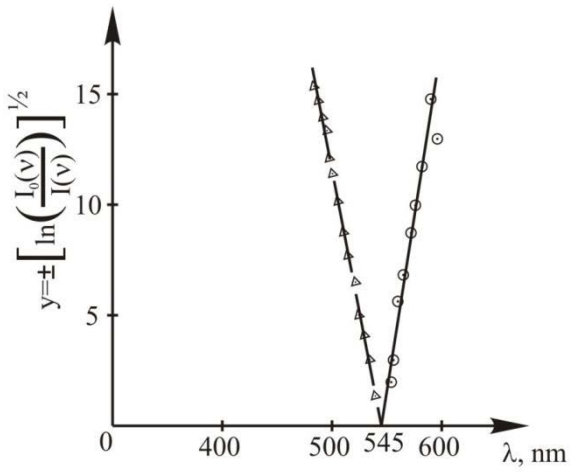

Fig.7. Dependence of energy coefficient B_e on excitation light wavelength.

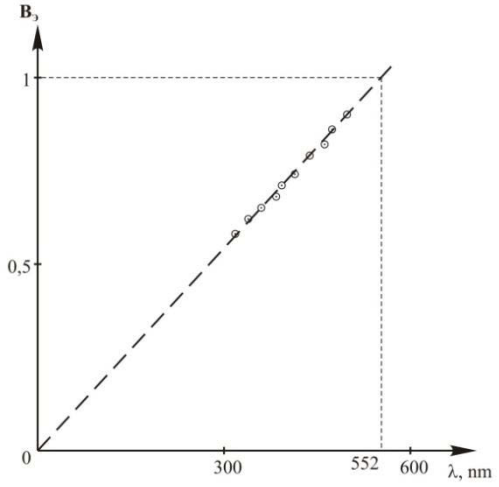

Fig.8 $y = \pm\left[\ln\left(\frac{I_0\nu}{I\nu}\right)\right]^{\frac{1}{2}}$ dependence on light wavelength at which the photoluminescence is observed. T=300K.

Indeed, as it is shown in [17], the expressions for PL energy efficiency when luminescence spectral composition in wide limits independent on wavelength or frequency of excitation light, has the following form:

$$B_e = \frac{h\int \nu W(\nu_{exc},\nu)d\nu}{h\nu_{exc}} = \frac{\nu}{\nu_{exc}} \qquad (2)$$

where ν is frequency average value in luminescence band, $W(\nu_{exc},\nu)$ is $h\nu$ quantum emission probability.

When emission probability doesn't depend on excitation light frequency (ν_{exc}) one can write. $W(\nu_{exc},\nu)_2 = W(\nu)$. In this case $B_e \sim \frac{1}{\nu_{exc}} \sim \lambda_{exc}$ (taking into consideration $\nu = \frac{c}{\lambda_{exc}}$) and we make the conclusion on linear dependence B_e on λ_{exc}. The expression (2) takes place when luminescence quantum efficiency is equal to unit: B_κ=1.

At $B_\kappa \neq 1$ energy efficiency B_e differs from expression (2) by B_κ multiplier for luminescent materials with PL spectra.

The processes taking place in luminescent materials are decribed in details in [13-17]. The spectrum form and quantum efficiency of luminescence don't depend on excitation light wavelength (Vavilov law). This takes place because of the fact that luminescent emission appears always from lower excited level irrespective of the fact which activator level was excited after absorption 300÷480nm [8,10,14].

On the base of experimental data shown on fig.5 PL energy efficiency B_e in nanocrystals $CaGa_2S_4:Eu^{2+}$ is obtained. The results for nanocrystals are shown on fig.6. According to Vavilov law, this figure shows that linear dependence between B_e and λ_{exc} exists in 320÷480nm region. As Vavilov mentioned, the dependence between B_e and λ_{exc} leads to simple empirical law $B_e = \kappa\lambda_{exc}$ where k is constant value, λ_{exc} is excitation light wavelength. Constant k is PL quantum efficiency: $B_\kappa = \kappa$. Fig.6 shows that extrapolation of dependence $B_e = f(\lambda_{exc})$ has the region for B_e from 0 up to 1. As it is above mentioned, experimental results for B_e and B_κ are between 320 and 480nm. At the same time the emission intensity strongly decreases that corresponds to excitation light wavelength above 480nm. The theoretical trend of curve $B_e = f(\lambda_{exc})$ is shown on fig.6 by dotted line. The extrapolation line $B_e = f(\lambda_{exc})$ to increase of λ_{exc} value crosses B_e axis in A point with coordinates (1 and 500nm). This confirms S.I.Vavilov's idea on the fact that PL energy efficiency can't be more than unity: B_e=1.

In temperature interval 10÷350K the measurement of PL spectrum full width at half maximum (FWHM) in Eu,Ca,Ba tiogallats shows that Huan Rice parameter S changes from 5 up to 10 [1-4]. This shows that in given materials the electrophonon interaction takes place and PL spectral dependence is described by Gaussian distribution [19].

$$I(h\nu) = \frac{1}{\sigma(2\pi)^2}\exp\left[-\frac{(h\nu - h\nu_0)^2}{2\sigma^2}\right] \qquad (3)$$

where $h\nu$ is excitation emission energy; $h\nu_0$ is photon energy corresponding to maximum in PL spectrum, σ is constant connected with squared half-width W(T) by following expression:

$$W(T)^2 = \sigma^2 8\ln 2 \qquad (4)$$

According to Gaussian distribution the experimental data represented for PL spectrum of $CaGa_2S_4:Eu^{2+}$ nanocrystal samples in $y = f(h\nu)$ coordinates have the form of line (fig.7) where $y = \pm\left[\ln\left(\frac{I_0(\nu)}{I(\nu)}\right)\right]^{1/2}$. The correspondence of PL spectrum to Gaussian distribution allows us

to define the energy position of intensity maximum and PL spectrum half-width with accuracy.

CONCLUSION

The excitation and emission spectra of nanodimensional crystals and volume crystals $Ga_2S_4:Eu^{2+}$ are investigated at temperatures 77 and 300K.

According to S.I.Vavilov law, it is shown that PL energy efficiency in interval 300÷480nm linearly increases when the excitation light wavelength increases. The maxima at 420, 440, 460, 485nm of wavelengths are revealed on excitation spectrum of $CaGa_2S_4:Eu^{2+}$ nanocrystals. The energy of given excitation light wavelengths effectively transforms into visible light energy.

The given work is supported of Science Development Foundation under the President of the Respublic of Azerbaycan (grant № EIF BGM -2 BRFTF -1-2012/2013- 07/02/1).

[1] *B.G. Tagiyev, S.A. Abushov, O.B. Tagiyev.* Journal of Applied Spectroscopy, vol.77, pp. 124-128 (2010) (in Russian).
[2] *B.G. Tagiyev, V.A. Jalilov, T.A. Gulmaliyev et al.* Inorganic materials, vol.28, № 12. pp.2269-2275, (1992) (in Russian).
[3] *I. Seishi, M. Tamao, N. Mamedov et al.* Jpn. J. Appl. Phys., vol. 36, pp.857-859 (1997).
[4] *C. Charter, R. Jabbarov, M. Jouanne et al.* J. Phys: Condens. Matter, vol. 14, pp.13693-13703 (2002).
[5] *P.U. Butagin.* Chemistry Successes, vol. 53, p.1769 (1984) (in Russian).
[6] *V.L. Levshin, I.V. Weiz* . JETP, vol. 20, №.5, p. 441 (1950) (in Russian).
[7] *A.M. Gurvich* Chemistry Successes, vol. 35, № 8, p. 1495 (1966) (in Russian).
[8] *A.A. Babushkin*, *P.A. Bajulin*, *F.A. Korolev*, *L.V. Levshin*, *A.R. Striganov, V.K. Prokofyev.* Spectral analysis methods. MSU, pp. 406-416 (1962) (in Russian).
[9] *V.P. Vasilyev.* Analytical chemistry, Book 2, Methods of physical-chemical analysis, Drofa, Moscow, (2004) (in Russian).
[10] *B.I. Stepanov.* Vavilov law. SPS, vol.58, №.1, p 3, (1956) (in Russian).
[11] *S.I. Vavilov.* Dependence of colour fluorescence intensity on light excitation wavelength. Composition, vol.1, article 8, pp. 105-117, (1954) (in Russian).
[12] *S.I. Vavilov.* Fluorescence output of clour solutions. Composition, vol.1, article11, pp.150-156; Notes about work of S.Valintiner and M.Ressiger "On fluorescence economy" article 14, pp.179-181 (1954) (in Russian).
[13] *U.P. Timofeyev, S.A. Fridman, M.V. Fock.* Light transformation. Moscow, "Science" 1985 (in Russian).
[14] *V.L. Levshin.* Emission of activated crystals. UPS, vol.43, (1951) (in Russian).
[15] *S.S. Solomin.* RAS USSR, vol. 31, p.741 (1941) (in Russian).
[16] *M.I. Epshteyn.* Spectral measurements in electrovacuum technique. Energy, Moscow, (1970).
[17] *E. I. Adirovich.* Some questions of crystal luminescence theory. State publishing of technical-theoretical literature, Moscow (1951) (in Russian).
[18] *V.V. Antonov-Romanovskii, M.I. Epshtain.* RAS USSR, vol. 64, p.483 (1949) (in Russian).
[19] *D. Curie, D.S. Perener.* Luminescence connected with deep levels. In book "Physics and chemistry of AB compounds" , "World ", Moscow, 1970, pp.334-371.

Recevied: 12.02.2015

THE INVESTIGATION OF COMPOSITE FILMS CONTAINING GaAs AND GaAs<Te> BY ROENTGENODIFFRACTOMETRIC METHOD

M.I. ALIYEV*, N.N. GADJIYEVA, G.B. AKHMEDOVA*, A.M. ALIYEVA***
**Institute of Physics of Azerbaijan NAS, 1041, Baku, Azerbaijan, G.Javid ave.,33*
***Institute of Radiation Problems of Azerbaijan NAS, 1041, Baku, Azerbaijan, B.Vakhabzade str.,9*
gunayehmedova12@gmail.com

The initial films HDPE and composite films on the base of high-density polyethylene and semiconductor fillers HDPE+GaAs and HDPE+GAS<Te> at room temperature are investigated by the method of roentgenodiffractometric analysis. The crystallinity (C) degree values of these samples are calculated. It is revealed that crystallinity degree value of composite films increases in 1,3 and 1,4 times (17-20%) correspondingly in the result of implantation of GaAs and GaAs<Te> micro-particles in polymer matrix. The obtained results are explained within framework of three-phase models and change of polymer permolecular structure at implantation of filler micro-particles (d-50μm) playing the role of additional centers of nucleus of crystallization.

Keywords: roentgenodiffractometry, HDPE, GaAs, GaAs<Te>, composite, permolecular structure, crystallinity degree.
PACS: 85.60.Pg; 78.20.e; 78.67.Bf; 78.70; Ck; 42.79.Wc.

INTRODUCTION

The obtaining of polymer compositions with interesting properties significantly depends on filler nature, particle dimension and its distribution character and degree of interaction between components. Usually, the new fillers lead to change of polymer matrix morphology. The composition materials obtained on the base of new fillers acquire the unique properties [1-2]. In this aspect the composites on the base of high-density polyethylene (HDPE) with semiconductor compounds GaAS and GaAs<Te> is of the special interest. This is caused by the facts that given semiconductors have the peculiar crystal and band structures and are perspective materials in microelectronics and optoelectronics [2-3]. HDPE-GaAs composite films are widely used in the capacity of neutron detector [4-5]. HDPE ($C_{2n}H_{2n+2}$) choice as polymer matrix is caused by well study of the given material [6-8]. Note that the information on composite study of HDPE-GaAs and HDPE-GaAs<Te> is practically absent in scientific literature. The similar investigations are firstly carried out by us; their results are presented in [9-10]. As these investigations show the change of optical-spectrometric and heat parameters are interconnected with the change of supramolecular structure (SMS) of polymeric matrix [9-10].

The present paper is the cycle continuation of these investigations and is dedicated to study of composite films HDPE-GaAs and HDPE-GaAs<Te> (filler content is 1-10 mass%), obtained by roentgenodiffractometric spectroscopy method. The given method allows us to see the structural changes caused by implantation of microparticles in polymer matrix composition and reveal the regularities connected with these changes [11-12].

EXPERIMENT TECHNIQUE

The homogeneous mixture is prepared from HDPE powders and GaAs and GaAs<Te> semiconductors (with particle dimensions ~50μm) by the way of mechanical mixing. Further, the homogeneous mixture is subjected to hot pressing at temperature T=413K with soaking during 15 minutes and is cooled up to room temperature during 30 minutes. The given method allows us to obtain HDPE films with uniform distribution of microparticles in polymer volume that is the necessary factor for optical and spectral investigations.

The distribution uniformity of microparticles in HDPE films is controlled by Fourier-IR absorption spectrum background. The thicknesses *d* of initial and composite films are equal to 50-100 μm. The content of introduced quantity of GaAs and GaAs<Te> microparticles is varied from 1 up to 10 mass%. The diffractograms of initial and composite samples are obtained on powder roentgen diffractometer D2 Phaser (Bruker). CuKα is the source and Ni filter is used. The values of crystallinity degree of investigated samples are calculated.

THE RESULTS AND THEIR DISCUSSION

The diffractograms of initial films HDPE (a), composite films HDPE +2%GaAs (b) and HDPE +GaAs<Te> (c) are given on fig.1. As it is seen from fig.1(a) PE initial films are characterized by the presence of series of reflexes: $2\theta=22^o$ and 24^o. The given lines are character lines of PE crystallinity (a).

The implantation of gallium arsenide 2 mass% into matrix composition leads to appearance of new strong lines 27^o and 45^o, comparatively weak lines $53{,}5^o$ and $72{,}5^o$ and also series of weak ones.

The new observable lines are related to GaAs(b). The same diffraction lines (reflexes) as in HDPE +GaAs composite the intensities of which are redistributed at doping of gallium arsenide in matrix content doped by tellurium 2mass% (c). The redistribution of diffraction lines (fig.2a,b) takes place with increase of implanted microparticle concentrations in polymer matrix composition from 2 up to 6 mass% and positions of these lines don't change. The strongest lines are: $2\theta=27;45$ and $53{,}5^o$.

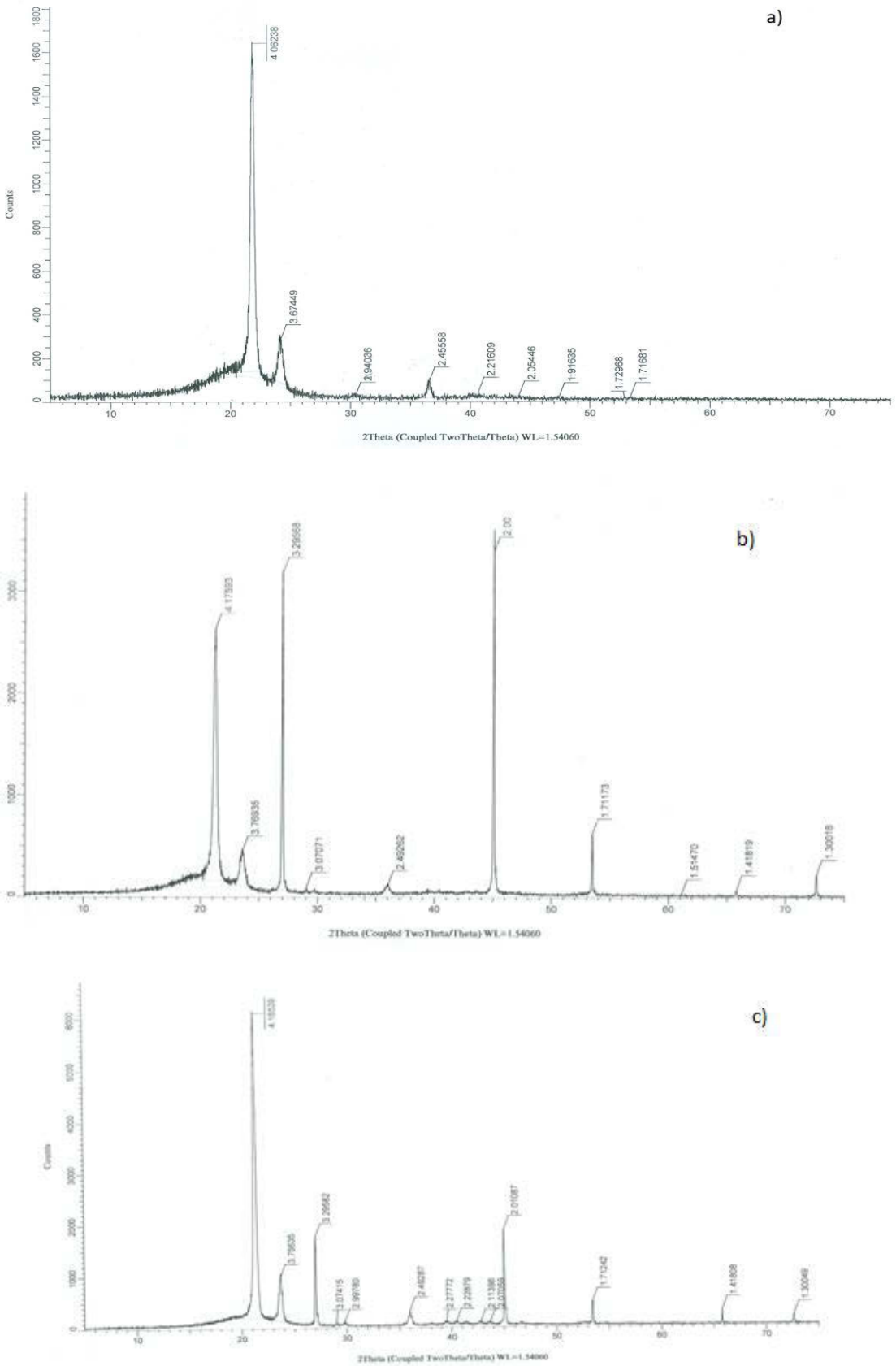

Fig.1. The diffractograms of PEHD (a), PEHD +2mass%GaAs (b) and PEHD +2mass%GaAs<Te> (c).

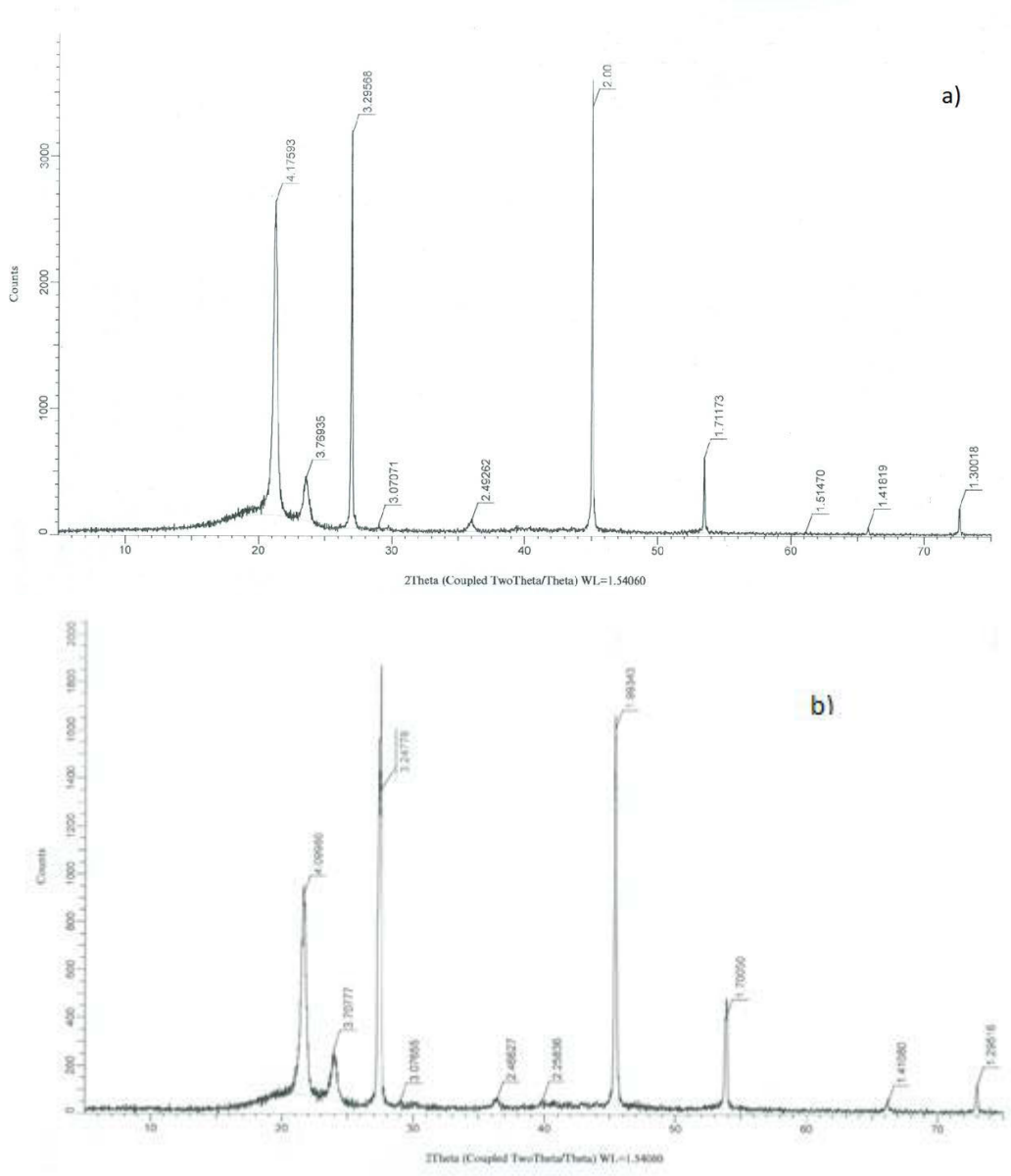

*Fig.2.*The comparative diffractograms of HDPE +GaAs 2 mass% (a) and HDPE +GaAs 6 mass% (b).

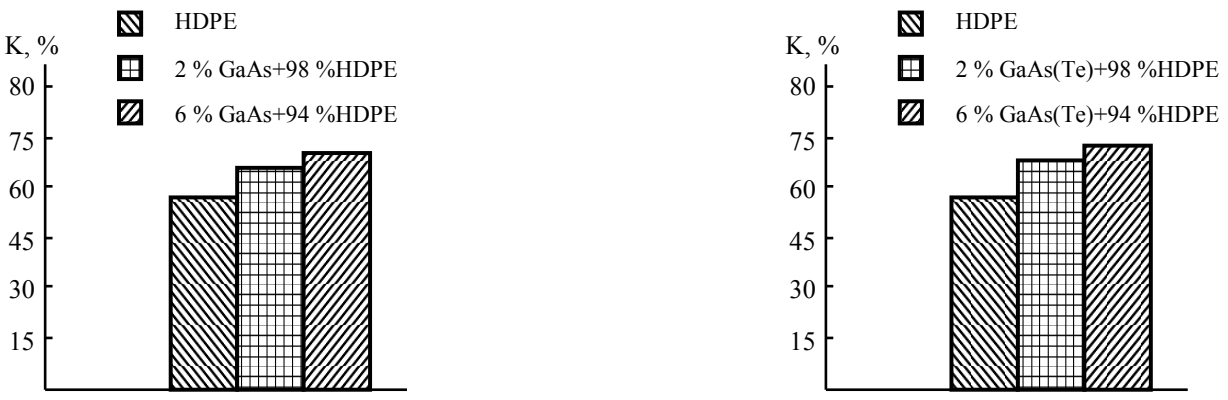

Fig.3. The histograms of crystallinity degree change HDPE +GaAs and HDPE +GaAs<Te> on addition concentrations.

The intensity change of HDPE crystal phase lines is significantly seen. The crystallinity degrees of HDPE initial films, HDPE +GaAs composite films (b) and HDPE +GaAs<Te> (c) are calculated on the base of given data by known program. It is established that the crystallinity degree of composite materials HDPE +GaAs relatively initial films maximally increases in 1,3 times (from 54 up to 71,4%) and for HDPE +GaAs<Te> composites increases in 1,4 times (from 54 up to 73,9%) with increase of concentration of additions. The observable changes are well agreed with data followed from Fourier-IR spectroscopic investigations [9]. The histograms of crystallinity degree redistribution on mass content of implanted microparticles of additions are shown on fig.3.

Thus, on the base of comparative roentgeno-diffractometric analysis it is established that crystallinity degree of composite films in comparison with crystallinity degree of initial films increases on value K =17-20%. The observable effects are probably connected with change of supramolecular structure (SMS) and polymer crystallinity degree (C) as GaAs и GaAs<Te> fillers with dispersivity 50μm in compositions with polyethylene play role of structure generators(these microparticles are nuclear crystallization centers) in crystallinity degree increase and in change of polymer supramolecular structure. Indeed, the well correlation is observed between Fourier-IR spectroscopic values and crystallinity degree ones. The crystallinity increase can take place because of formation of third transient phase according to three-phase model of supramolecular structure (SMS) of amorphous-crystalline polymer consisting of mainly straightened chains (SC) proposed in [12]. According to roentgen data SC can have the three-dimensional structure with periodicity λ=50-60нм [13]. SC are inherent part of high-oriented PE. The value λ for PE fibers corresponds to length of trance-sequences in lamel crystalline regions. Probably, GaAs 2-6 and GaAs<Te> 2-8 mass % microparticle concentrations in PE content lead to SC increase quantity in PE transversal crystalline layer. This can be caused by the fact that GaAs и GaAs<Te> microparticles are centers of additional crystallization at these concentrations. At increase of filler microparticle concentrations in PE content bigger than 6 mass% the cluster dimensions for GaAs and GaAs<Te> begin strongly to exceed the SC periodicity value that is revealed in decrease of relative degree of periodicity.

Probably, the microparticle dimension increase prevents the chain straightening and crystallization process. The filler concentration increase leads to cluster-formation, decrease of surface energy and stabilization up to completion of polymer crystallization processes.

---

[1] *M.F. Galikhanov, D.A. Eremeev, R.Y. Deberdeev.* Russian Journal of Appl.Chem, 2003, v.76, №10, pp. 1651-1654.

[2] *L.I. Traxtenberq, Q.N. Qerasimov, V.K. Potanov.* Vestnik Moskovskoqo universiteta, 2001, tom 42, №5, s.325-331. (In Russian).

[3] *Q. Efendiev, N,N, Qadjieva, T.M. Ilyasli, R.F. Abbasova, F.F. Axyaev.* Jurnal prikladnoy pektroskopii. 2006, tom 73, № 3, ss.408-410. (In Russian).

[4] *D.S. McGregor,R.T.Klann, H.K. Gersch, Yong Hong Yang.* Thin-film –coated bulk GaAs detectors for thermal andv fast neutron measurements,Nuclear Instruments and Methods, A466, 2001, pp.126-141.

[5] *D.S.McGregor,S.M.Vernon,H.K.Gersch,S.M.Markham, S.I.Wojczuk.* D-R Wehe, Self –biased Boron-10 coated high purity epitaxial GaAs thermal neutron detectors,IEEE Transactions on Nuclear Science, NS-47, 2000, pp1364-1370

[6] *E.M. Qodjaev, A.M. Maqerramov, Sh.A. Zeynalov, S.S. Osmanova, E.A. Allaxyarov.* Elektronnaya obrabotka materialov. 2010, №6, s.91-96. (In Russian).

[7] *Q.A. Mamedov, E.M. Qodjaev, A.M. Maqerramov, Sh.A. Zeynalov.* Elektronnaya obrabotka materialov.2011, tom 47, №6, s.94-98. (In Russian).

[8] *E.M. Qodjaev, A.M. Maqerramov, S.S. Osmanova,M.A. Nuriyev, E.A. Allaxyarov.* Elektronnaya obrabotka materialov. 2007, № 2, s. 84-88. (In Russian).

[9] *M.I. Aliev, N.N. Gadzhieva, G.B. Ahmadova.* Fourier –IR study of the high –density polyethylene composites with semiconductor fillers GaAs and GaAs<Te>. International Journal of Composite Materials, 2014(1), pp.1-3.

[10] *M.I. Aliev, N.N. Gadzhieva, G.B. Ahmadova.* Transactions of Azerbaijan National Academy of Sciences (physics and astronomy), 2014, v..34, №,2, pp.43-46. (In Russian).

[11] *Q.P. Okatova, N.A. Svidunovich.* Ros. Xim.jurn. 2006, t.L, № 1, s. 68–70. (In Russian).

[12] *A.A. Lunkova, S.D. Kaloshkin, M.B.Qorshenkov, V.V. Cherdintsev.* Elektronnoe nauchnoe-tekhnicheskoe izdanie Nauka i Obrazovanie, 2012, №10. (In Russian).

[13] *A.M. Maqerramov.* Baku, «Elm», 2001, 327s. (In Russian).

Recevied: 03.02.2015

HDPE+Fe_3O_4 MAGNETIC POLYMER NANOCOMPOSITE TECHNOLOGY AND INVESTIGATIONS OF ITS STRUCTURE BY SEM

P.B. ASILBEYLI [2*], M.A. RAMAZANOV [1,2], H.S. IBRAGIMOVA [2]

Baku State University[1], Institute of Physics of ANAS[2]

AZ1143,G.Javid ave.,33, Baku, Azerbaijan

e-mail: asilbeyli@mail.ru

The synthesis methods of composite nanomaterials on the base of HDPE polymer matrix and Fe_3O_4 magnetite nanoparticles are developed. The optimal conditions and synthesis process parameters (temperature, concentration of metal-containing compound, time and temperature-time mode of crystallization) influencing on phase composition, nanoparticle dimensions and physicomechanical properties as a whole are established.

SEM-investigations of HDPE+ Fe_3O_4 nanocomposites are carried out. The possibilities of scanning electron microscopy and microroentgenospectral analysis being in investigation methods of material microstructure, definition of quantitative element composition and map construction of element distribution on analytic complex example are shown.

Keywords: nanocomposites, magnetic polymer.
PACS:79.60.Dp; 78.66.Li; 78.30.Am

INTRODUCTION

As a result of gathered scientific data and their analyses it is established that nanocomposite technology can be divided into two methods. The first method is nanocomposite assembly going from bottom with stay of phase increase with the help of surface-active substance. The grinding of massive substance samples takes place in second place. At particle dimensions 1÷20 nm the composite surface has the big excess energy that's why the big attention is paid to nanoparticle stabilization process. As a result of interaction of nanoparticles with inert atmosphere substance, in surface layer the appearance of modified phase is possible. The chemical synthesis of magnetic nanoparticles is carried out by two general methods: the obtaining of particles, the surface of which is covered by surface-active substances or ligands (ex situ), or method where their "hard" stabilization in matrixes (in situ) takes place simultaneously, i.e. nanoparticle stabilization takes place in process of their obtaining. The product, which is constant by its properties, forms in output. In the first method the possibility to operate with nanoparticle surface, for example, the ligand substitution or further surface modification, obtaining of particle monolayers and etc. is saved. The advantage of second method is in the fact that we usually deal with nanomaterial for which the nanoparticle collective properties are especially important. This method we use in our work. The composite material class formed by nanoparticles and organic polymers, as they are attractive ones by technological simplicity, presents the especial interest in this aspect. Because of their plasticity, such materials demonstrate the perspective electric, optic, magnetic and mechanical properties caused by not only individual peculiarities of nanoparticles and polymers but by interactions of interfaces of two materials different by its nature which are inorganic/organic in supramolecular scale.

The modern state of magnetic record technology confirms that transition to magnetic nanomaterials allows us to increase the density of record information in 10^3-10^4 times [1,2]. That's why the development of synthesis methods of polymer nanocomposites with magnetic component, investigation of mechanism of their formation and stabilization, the study of their structure has the big meaning for obtaining of new information on substance magnetic property peculiarities in nanostate. The use of polymer matrixes of different types allows us easy regulation of the morphology of such systems and especially the particle dimension and distance between them changing the synthesis conditions [3]. The wide range of structural characteristic changes presents the well possibility for regulation of magnetic interactions between particles of nanophase, study of this interaction influence and dimensional factor on nanosystem magnetic properties.

THE EXPERIMENT TECHNIQUE AND SAMPLE PREPARATION

The nanoparticles and composites with Fe_3O_4 nano-particle addition are obtained by following way in present paper. The magnetic liquid containing the ferric oxide nanoparticles by dimension 3-5nm is obtained by chemical condensation method (colloidal solution of Fe_3O_4 magnetite in water). Further, Fe_3O_4 nano-particles are added in 2% solution of granuled high-density polyethylene (HDPE by 293-285D mark) in carbon tetrachloride CCl_4 and mixture is mixed at temperature 373K up to emulsion formation. After water solution addition HDPE containing Fe_3O_4, which later is dried in vacuum box, isolates. All nano-composite samples are obtained by the same above mentioned method in different concentrations of Fe_3O_4 necessary for us and all described technological factors of their obtaining are supported constant ones for study of concentration change influence of initial reagents on obtained sample properties. The obtained non-transparent film samples which are separeated from Petri cups, are treated by hot pressing method at melting point of polymer matrix under pressure 15Mpa during 10 min with further cooling in different temperature-time crystallization modes: rapid cooling (RC) at temperature decrease rate

β=2000 grad/min („tempering in liquid nitrogen medium“) and slow cooling (SC) at rate β=4 grad/min not without pressure.

Further, HDPE+Fe_3O_4 nano-composite samples in film forms are obtained from above mentioned films with the help of hydraulic press with heated molds at hot pressing. The choice of technological pressing conditions, such as pressure, temperature and enduring time in material melted state is necessary condition at sample obtaining of polymer nano-composite films with different morfology and structural pecularities. The researchers often have methodical difficulties at choice of methods and techniques of investigations by device type and etc. at studyof structural state [4-6]. It is known that scanning electron microsope (SEM) allows simultaneously to research the dimensions and form of nano-particles, distribution of nanoparticles and phases by dimensions, to obtained the phase composition and distribution of chemical elements by its square and square of investigated sample, chemical heterogeneity by section square and also obtain the object image in wide range of enhancement in secondary and reflected electrons. The samples of magnetic polymer nanocomposite HDPE+ Fe_3O_4 in different concentrations 5, 10, 15, 20 vol.% Fe_3O_4 are the investigation objects of SEM by JSM-7600F mark (“Jeol”, Japan).

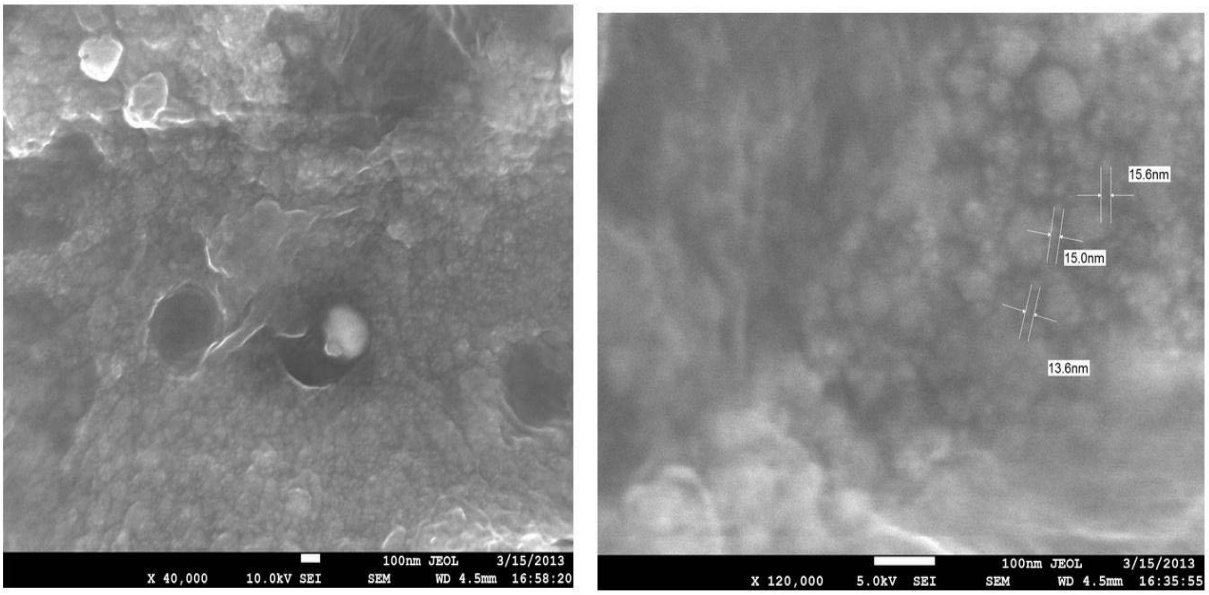

a) –x40 000 b) – x120 000

Fig. 1. a) is nanocomposite surface structure HDPE+10 vol.% Fe_3O_4 (SC); b) is form and dimensions of Fe_3O_4 in nanocomposite polymer matrix

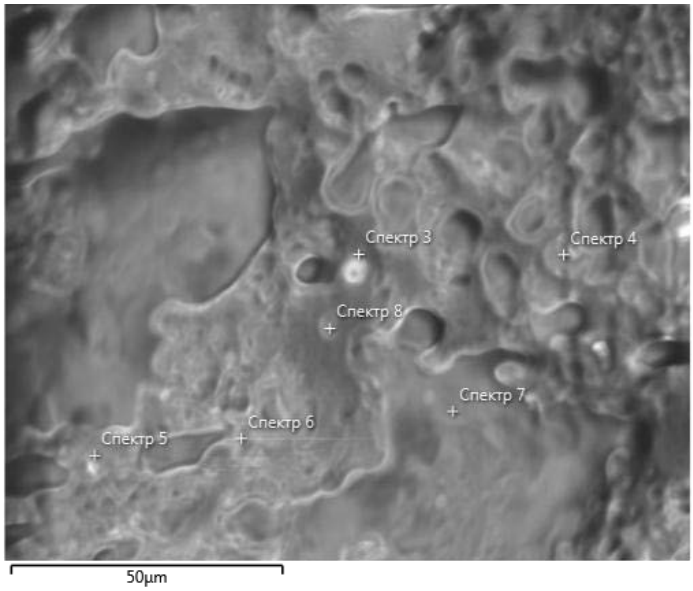

Fig.2. Energy-dispersion microroentgenospectral analysis of nanocomposite HDPE+10 vol.% Fe_3O_4 (SC).

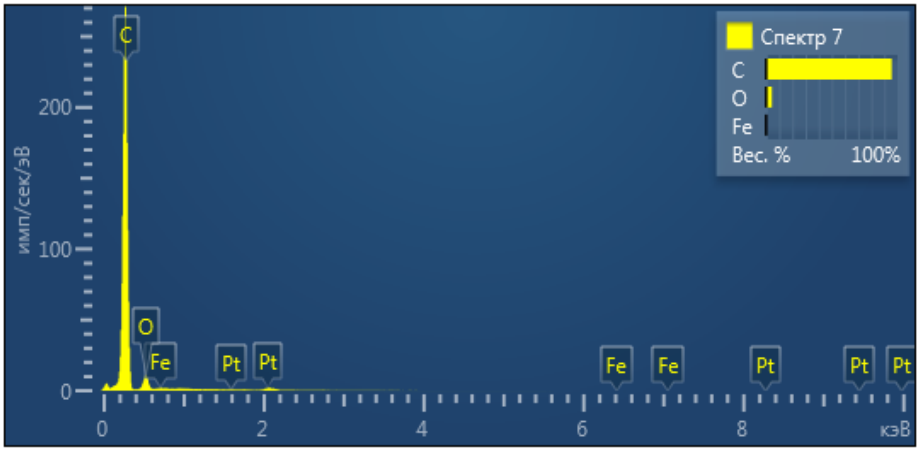

Fig. 3. General form of roentgen spectrum lines showing the element presence in point 7.

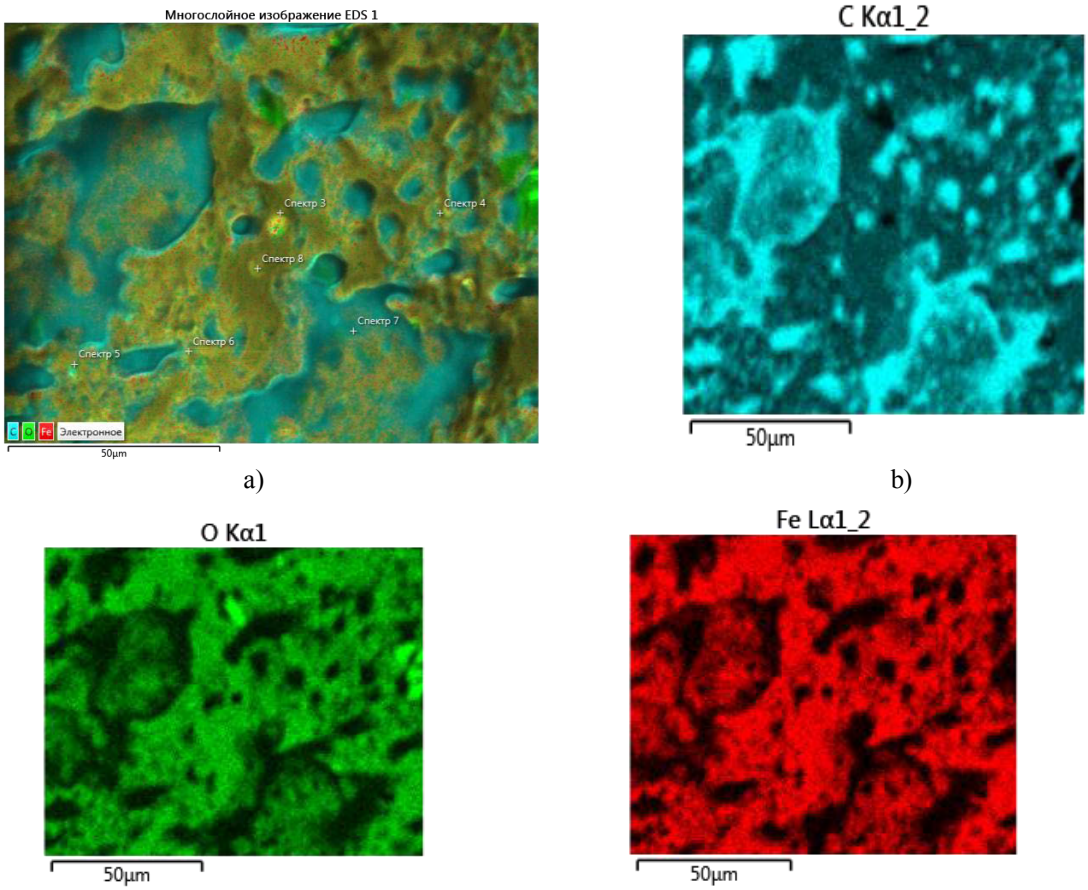

Fig. 4. Many-layered image of HDPE+10 vol.% Fe_3O_4 (MO) nanocomposite sample (a); mapping on this region on C (b), O (c), Fe (d)

RESULTS AND THEIR DISCUSSION

With the help of scanning electron microscopy it is established that magnetite nanoparticles are uniformly distributed in polymer matrix and nanoparticle sizes is 12-28nm in dependence on magnetite nanoparticle concentration (see fig.1). Also, Fe_3O_4 nanoparticle dimensions change with variation of temperature-time mode of polymer crystallization [7-9]. It is known that there are qualitative and quantitative roentgenospectral microanalyses. The quantitative microanalysis is necessary for quantitative determination of element concentration in sample. The qualitative microanalysis allows us to define what elements present in sample. The data of microroentgenospectral analysis can be represented in the form of standard protocols consisting of image of sample microstructure investigation region, table data in height or atomic ratio, spectra and histograms. The microstructure and phase element composition are investigated on sample of HDPE+10 vol.% Fe_3O_4 (SC)

nanocomposite. The sample microstructure investigations are often accompanied by microroentgen analysis, character peculiarity of which is locality: maximal excitation region is equal to 1 μm. This allows us to obtain the information on sample chemical composition in direct chosen region of microscopic dimensions. The microroentgenospectral analyses are carried out with use of energy-dispersion spectrometer in the use mode of secondary electron signals and electron backscattering. The accumulation of whole spectrum takes place in case of energy-dispersion spectrometer, that's why the qualitative analysis is automatically carried out at any measurement. The energy-dispersion spectrometer allows us to carry out the quantitative roentgen microanalysis with choice of analyzed given step region spectra: in the point, on square, on line (see Fig.2).

The quantitative element composition of six point spectra allows us to establish that bright phase consists of carbon (42,53 weight %), oxygen (40, 24 weight %), iron (17, 23 weight %) and dark one consists of carbon (100 weight %). The general form of roentgen spectrum lines showing the element presence in dark phase of point 7 is given on fig.3. The element distribution mapping on surface is carried out for confirmation of phase element composition (see fig.4a, b, c, d). If we impose the chemical element (see Fig.4b, c, d) distribution maps on microstructure (see fig.4a), then we obtain that bright phases consist of three elements C, O, Fe, dark ones consist of C only.

CONCLUSION

Thus the samples of polymer magnetic nano-composites HDPE+Fe_3O_4 obtained firstly by chemical methods, and then by hot pressing method in hydraulic press in different temperature-time modes of crystallization and different content of magnetite nanoparticles. Such films with high content of nanoparticles give the new possibilities for magnetic system formation with high density recording and information storage. Also the possibilities of scanning electron microscopy and microroentgenospectral analysis consisting of investigation methods of material microstructure, determination of quantitative element composition and element distribution map construction on example of analytic complex are shown.

[1] *Yu.A. Boykov, V.A. Danilov.* JTF, 2010, t. 80, vip. 8, s. 109-114. (In Russian).

[2] *J.P. Bucher, L.A. Blooméeld Bloomfield.* Int. J. Mod. Phys., 1993, v. B7, p. 1079.

[3] *D.K. Kim, M. Mikhaylova, Y.Zhang, M. Muhammed.* J. Chem. Mater, 2003, v. 15(8), p. 1617-1625.

[4] *D. Brandon, U.Kaplan.* Mikrostruktura materialov. Metodi issledovaniya i kontrolya. M: Texnosfera, 2004, 384 s. (In Russian).

[5] *Yu.A. Bikov, S.D. Karpuxin, M.K. Boychenko i dr.* Rastrovaya elektronnaya mikroskopiya i rentgenospektralniy analiz. Apparatura, printsip raboti, primenenie. Elektr. Dan. M: MQTU im.N.E. Baumena, 2003. (In Russian).

[6] *M.M. Krishtal, I.S. Yasnikov, V.I. Polunin i dr.* M: Izd-vo Tekhnosfera, 2009, seriya «Mir fiziki i tekhniki» II-15, 208 s.

[7] *M.A. Ramazanov, P.B. Aqakishieva, S.A. Abasov, R.A. Ali-zade.* J. Fizika, 2007, №5, s. 47-49. (In Russian).

[8] *M.A. Ramazanov, P.B. Aqakishieva, S.A. Abasov.* Plasticheskie massi, 2008, Moskva, № 10, s. 14-16. (In Russian).

[9] *M.A. Ramazanov, R.A. Ali-zade, P.B. Agakishieva.* Digest Journal of Nanomaterials and Biostructures, July-September 2010, v.5, №3, p. 727-733.

Recevied:05.12.2014

INVESTIGATION OF THE PERFORMANCE OF ALPHA PARTICLE COUNTING AND ALPHA-GAMMA DISCRIMINATION BY PULSE SHAPE WITH MICRO-PIXEL AVALANCHE PHOTODIODE

G. AHMADOV[1,3*], Z. SADYGOV[2,3], E. JAFAROVA[2], F. AHMADOV[1], R. MADATOV[1], R. MUKHTAROV[5], A. OLSHEVSKI[3], A. SADIGOV [1], F. ZERROUK[4]

[1]Institute of Radiation Problems of ANAS, Baku, Azerbaijan,[2]Institute of Physics of ANAS, Baku, Azerbaijan,[3]Joint Institute for Nuclear Research, Dubna, Russia,[4]Zecotek Photonics Pte, Ltd., Vancouver, Canada, [5]Azerbaijan National Academy of Aviation, Baku, Azerbaijan.
[*]ahmadovgadir@gmail.com

Being capable measuring small lights gives possibility to use micro-pixel avalanche photodiodes (MAPD) with scintillators. We show two prototypes to use MAPD with and without scintillators as alpha and gamma counters in this paper. First prototype is to use two MAPD. One for detecting alpha particles and closer to it second one with a thin plastic scintillator for detecting gamma rays. Second prototype is called two-layers configuration in which used only one MAPD but two scintillators with different decay times. One can distinguish alpha particle and gamma ray events by using pulse shape discrimination techniques in the two-layer configuration.

Keywords: micropixel avalanche photodiode; scintillator; counter, pulse shape discrimination.
PACS: 07.77.-n; 07.77.-Ka; 29.40 Wk; 85.30 De; 85.60 Dw.

INTRODUCTION

Micro-pixel avalanche photodiodes are powerful tools for an optical readout. Their gain is about ~10^5-10^6, photon detection efficiency 15–30%, up to15000 pixel/mm^2 high pixel density and low operation voltage (~90V). Detailed information about Micro-pixel Avalanche Photo Diodes and their parameters can be found [1, 2]. MAPD and its modifications are widely used in the fields such as astronomy, high energy particle physics, medicine, spectroscopy, environmental measurements et.c. [2-8].

COUNTER DESIGNS

a. Two MAPD and 3x3x1 mm plastic scintillator were used in the fist prototype. The MAPD without scintillator is for alpha particle detector. It is completely insensitive to gamma rays due to small active region (4mkm). Gamma photon detection is usually performed with scintillation detectors. Therefore the second MAPD with the plastic scintillator (p-terphenil) was placed very close to the first one to register gamma rays. The MAPD with scintillator is also sensitive alpha particles. Experimental setup is shown in Fig.1 (a) for testing the prototype.

b. Only a MAPD and two scintillators were used in the second prototype (the two-layer configuration). The scintillators were BGO (Bismuth germinate Bi4Ge3O12) and p-terphenil (C14H18) plastic which decay times are 300ns and 3.7 ns, consequently. Plastic scintillator thickness was very thin (1mm) but it is enough to stop alpha particles since the range of 6 MeV alpha particles in plastic is around 50 μm [9]. Therefore all of the energy of the alpha particles is absorbed in plastic scintillator (the first layer). Besides alpha particles low energy gamma photons are also absorbed in the first layer due to the thickness of the plastic scintillator. 3x3x10 mm BGO scintillator was used for detection penetrated gamma rays through the first layer. Experimental setup is shown in Fig.1 (b) for testing the prototype.

EXPERIMENTAL SETUP AND METHODS

Experimental setup is shown in Fig.1 for testing the prototypes. The MAPD was biased by Keithley high voltage supply via RC circuit (390kOm resistor and 30 nF capacitor) for noise suppression. Amplifier with a 25 voltage gain was used to amplify signal from the MAPD. The signals from the MAPD were digitized using a 5GS/s DRS-4 digitizer. The digitized signals were fed to personal computer (PC). The digitized data were processed offline using ROOT. It was used a subtraction method to find number of alpha and gamma events in the first prototype. If assumed that N_g is event number of gamma photons and N_a alpha particles then event numbers are N_a on the first detector, but N_a+N_g on the second. Event numbers corresponding to alpha particles and gamma rays were found from their difference. Because N_a is always known (the bare MAPD is insensitive gamma rays). Am^{241} alpha and Cs^{137} gamma ray radioactive sources were used for testing the both detectors. The registered alpha particle events by the both detectors were shown in Fig.2.

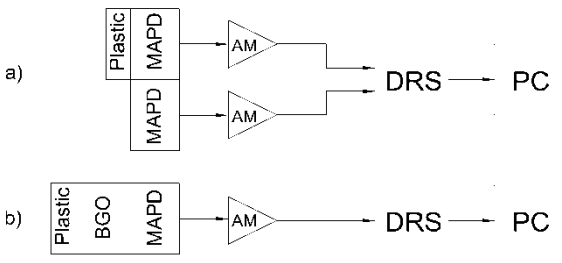

Fig.1. Experimental setup.

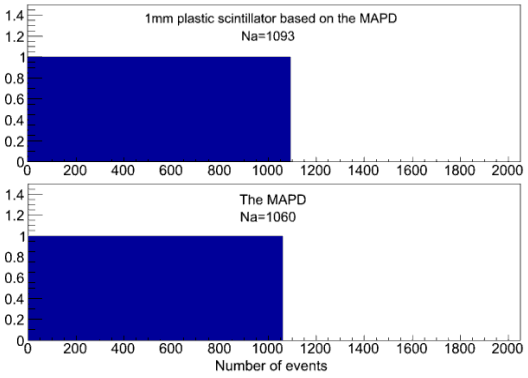

Fig 2. Alpha particle events from the plastic scintillator based on MAPD (up) and from the MAPD (bottom).

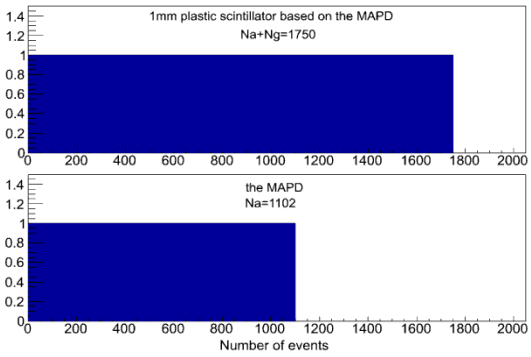

Fig 3. Alpha-gamma events from the plastic scintillator based on MAPD (up) and alpha particle events from the MAPD (bottom).

It is shown that from Fig.2 the both detectors register about same events. The experiment was repeated for several times and every time the registered events were close to each other with 5% uncertainty. Number of events from Cs^{137} and Am^{241} sources was shown in Fig. 3. Counted events by the MAPD for two cases were about same as shown from Fig.2 and Fig.3. One can calculate number of gamma events from difference of the both detectors' responses. Gamma ray events were 650 in the experiment. This result was also tested with just Cs^{137} gamma ray source and the registered events were close to each other with 5% uncertainty.

The pulse shape discrimination technique was used for the second prototype. Since the decay time of BGO is 300 ns and of plastic scintillator is 2.4 ns, and then one can easily discriminate long and short signals. Output signals from MAPD with BGO and plastic scintillators are shown in Fig. 4. Because of the limitation of the band width of the amplifier, the measured decay time is around 80 ns for plastic scintillator.

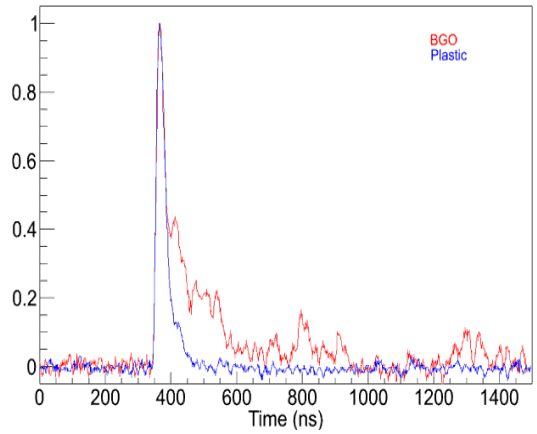

Fig. 4. Normalized output signals from MAPD with BGO and plastic scintillators.

Pulse height differences between the scintillators that complicate signal processing were solved using normalization. Signals from both detectors were normalized to 1 for exact discrimination. It makes discrimination easy and prevents to confuse alpha and gamma events. The integration windows were selected digitally by PC.

CONCLUSION

In this work a alpha particle and gamma ray counting performance of MAPD diode without scintillators and in combination of plastic and BGO+ plastic scintillators was investigated. Obtained results showed the detection performance of the MAPD diode in combination plastic scintillator was about same as conventional semiconductor detectors. The pulse shape discrimination technique was studied by MAPD diode in combination of BGO+plastic scintillators too. The large differences between scintillators decay times allowed making discrimination easy and preventing to confuse alpha and gamma events.

This research was supported by SOCAR grant.

[1] http://www.zecotek.com
[2] *Z. Sadygov et al.,* Nuclear Instruments and Methods in Physics Research A 610 (2009) 381–383
[3] *I.M. Zheleznykh, Z.Ya. Sadygov, B.A. Khrenov, et al.,* 30TH INTERNATIONAL COSMIC RAY CONFERENCE, 2008, Volume 5, p.1589-1592
[4] *Z. Sadygov et al.,* PoS(PhotoDet 2012)037
[5] *M. Golubeva et al.* Nuclear Instruments and Methods in Physics Research A 610 (2009) 366–369
[6] *N.V. Anfimov et al.* Physics of Particles and Nuclei Letters, 2012, Vol. 9, No. 9–10, pp. 758–761.
[7] *E. Guliyev et al.* ArXiv:1302.0278 2013
[8] *F. Ahmadov et.al.* Functional materials 20, №3, 2013.
[9] SRIM

Recevied:16.01.2015

SYNTHESIS OF $SrAl_2O_4:Eu^{2+}$ BY COMBUSTION METHOD AND INVESTIGATION ITS LUMINESCENCE PROPERTIES AT VARIOUS TEMPERATURES

S.A. MAMMADOVA[1], A.B. HUSEYNOV[2], T.Y. ORUCOV[1]
G.M. Abdullayev Institute of Physics, Azerbaijan NAS, Baku, Azerbaijan[1]
Research and Devolopment Center for High Technologies, Ministry of Communications and İnformation Technologies[2]

Safer and more energy effective Combustion synthesis method yields homogenic, stable phase and dimension phosphors and in contrast to more conventional solid-state reaction - a process that takes just 5-10 minutes. In order to get information on the crystal structure, X-ray diffraction analysis of the obtained luminescent material was conducted. The optical properties were explored by measuring emission and excitation spectra at room, low and high temperatures. We also have measured afterglow properties of these nanophosphors and compared their afterglow time with the results in literature.

Keywords: nanophsophor, combustion method **.**
PACS: 33.50.-j, 33.50.D.

1. INTRODUCTION

Phosphors are the most important materials in lighting. In our work we used oxide based phosphor - $SrAl_2O_4:Eu^{2+}$ (1%) doped with divalent europium ion because of its high brightness, high chemical and thermal stability and low toxicity properties [1]. In this work we obtained these oxide phosphors by combustion method, as by this method oxide phosphors are prepared in a safer, energy-efficient way and in a short period of time [2].
Divalent Eu^{2+} is a widely applied rare earth element, which gives a very intense and broad emission band in the visible region [3]. Inter-configurational electronic $f^7(8S_{7/2})$-f^6d transition causes broad emission band. Unlike 4f electrons the 5d electron is not shielded by the $5s^25p^6$ electrons, so their energy levels are split by the crystal field into t_{2g} and e_g components. At room and high temperatures there is only one broad emission band, but at low temperatures (e.g. 77-150K), emission spectrum is split into two bands. There are a lot of hypotheses for explaining this situation.

2. EXPERIMENTAL SECTION

All reagents were commercially purchased and used without further purification. For the synthesis, stoichiometric amounts of $Sr(NO_3)_2$ (99,99%), $Al(NO_3)_3 \cdot 9H_2O$ (99,99%), $Eu(NO_3)_3 \cdot 6H_2O$ (99,99%), $CO(NH_2)_2$ (99,3%) and H_3BO_3 (99,9%) were dissolved together in 20ml of deionized water to obtain a transparent solution. Small amount of boric acid was used as flux and urea was used as fuel [4, 5].

The components were mixed together and the solution was stirred using a magnetic bar at 70^0C for two hours. And in every 15 minutes the temperature of the solution was raised by 10^0C up to 130^0C. We got white viscous gel. The gel was placed in a preheated muffle furnace at 600^0C. At this temperature the solution evaporated, generating large amounts of gases, e.g. oxides of carbon and nitrogen. The combustion process lasted for about 5 to 10 minutes and resulted in white ash. At the next step, the precursor was annealed at 1000^0 C for 1 and 2 hours under an Ar /H_2 reductive atmosphere for the purpose reducing Eu^{3+} to Eu^{2+}.

Photoluminescence (PL) excitation and emission spectra were recorded between 77 and 350K on the FS 920 fluorescent spectrometer (Edinburgh Instruments) equipped with a Hamamatsu R928P red-sensitive photomultiplier (wavelength range from 200 to 850 nm). An Oxford Optistat CF cryostat was used to cover a measurement temperature range from 4 to 500K and to record the TL properties.

X-ray diffraction patterns were recorded using a Bruker 5000 diffractrometer in standard θ-2θ geometry using Cu Kα radiation.

3. RESULTS AND DISCUSSION

3.1 XRD analysis

Fig.1 shows the XRD of $SrAl_2O_4:Eu^{2+}$ (1%). From this X-ray diffraction analysis we can tell that our sample is not absolutely mono-phase. One of those is the main monoclinic $SrAl_2O_4$ phase and the other one is orthorhombic $Sr_4Al_{14}O_{25}$ phase. But there are no any lines of combination of other elements. It means that all nitrates, boric acid and urea were dissolved and during 5-10 minutes the combustion process absolutely finished. This proves once again that combustion method is really energy effective method.

3.2. PL properties of $SrAl_2O_4:Eu^{2+}$

The photoluminescence spectra of $SrAl_2O_4:Eu^{2+}$ was observed at different temperatures (77-400K). At room temperature (T=300K) we observe one symmetric broad band centered at 517 nm (FWHM=100 nm). This emission is characteristic for 5d-4f transitions in divalent europium. But at low temperatures (77, 150K) emission spectrum is split into two bands. These two bands are centered at approximately 445nm and 521 (FWHM= 79nm) at 77K; 442 nm and 521 nm (FWHM= 80nm) at 150K.

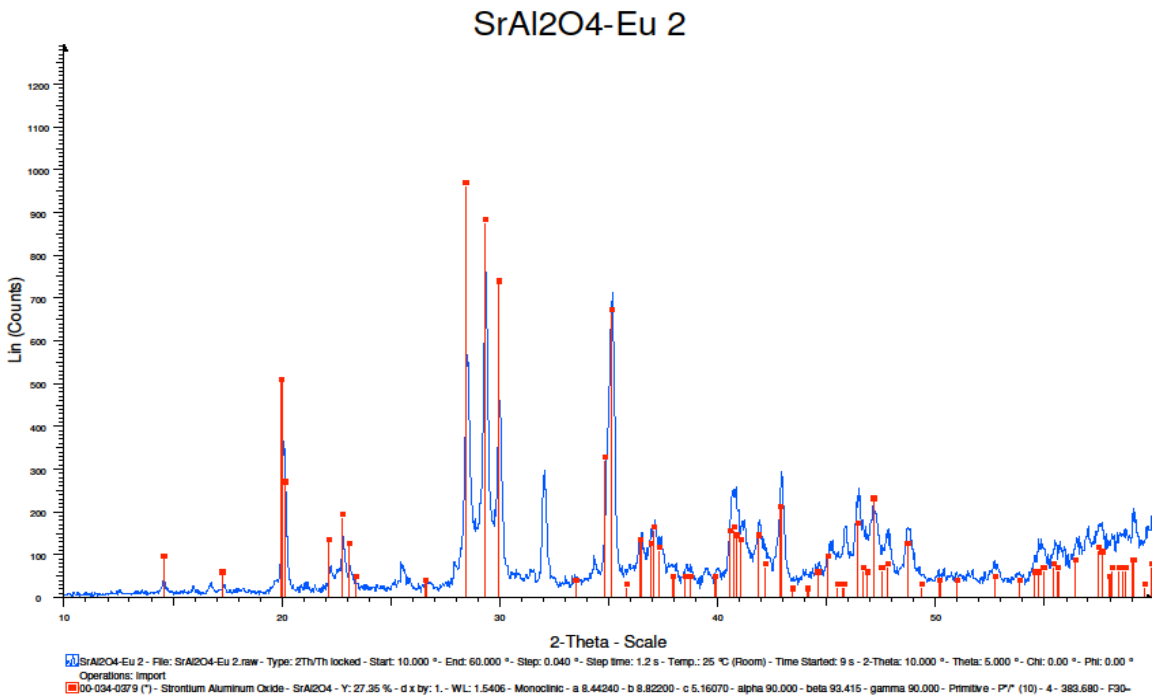

Fig 1. XRD for $SrAl_2O_4:Eu^{2+}$

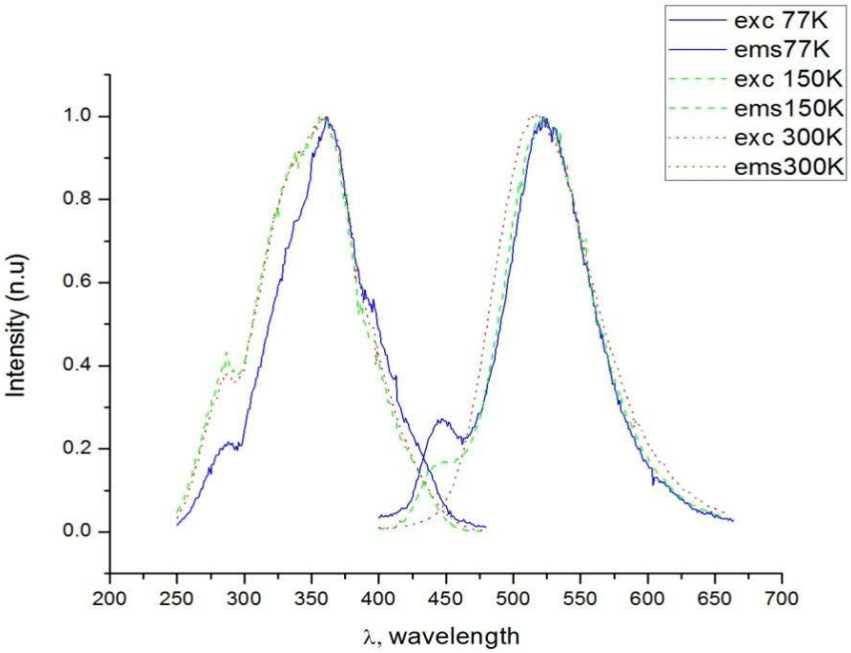

*Fig. 3.*The excitation and emission spectra of $SrAl_2O_4$: Eu^{2+}at different temperatures.

As shown in the figure 3 with increasing temperature the intensity of the blue emission band decreases and only green emission band remains. There are a lot of hypothesis to explain this situation. For example Clabau et al. explained this situation with charge transfer from level of $4f^7$ configuration to the valence band associated with a holedetrapping mechanism [6]. Other two hypothesis are associated with crystal structure of $SrAl_2O_4:Eu^{2+}$, which has a three-dimensional network (fig. 4) formed by corner sharing AlO_4tetrahedra with the Sr^{2+} ions in its a-, b-, c-directed channels. The Eu^{2+} ions replace the Sr^{2+} ions in such lattice in both seven-coordination sites (Sr1 and Sr2 , C1 site symmetry for both) since the average Sr-O distances are similar (2,695 and 2,667Å). Plus, Eu^{2+} and Sr^{2+} ions have very similar ionic sizes (1.20Å and 1.21Å, respectively).Poort at .all

explained this situation like that: There are two nonequivalent strontium sites with different coordination numbers in the $SrAl_2O_4$ crystal [7]. So the distances between the strontium ion and its neighboring oxygen ions are different for these strontium sites.

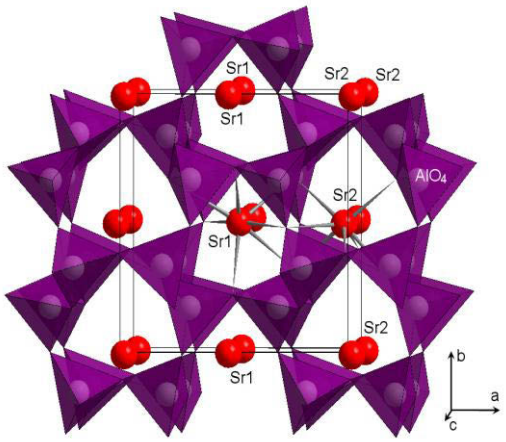

Fig. 4. Crystal structure of $SrAl_2O_4$ activated with Eu^{2+} ions.

If we look along the a axis, we can see that the oxygen ions are close to one Sr1 site, but far from other Sr2 site. So at the first site there is no any preferential orientation of *d* orbitals. But in the second case, because of the large distance between negative charges and Sr2 site, there is a preferential orientation of *d* orbitals present. Hence at low temperatures there are two emission bands in $SrAl_2O_4:Eu^{2+}$ spectra [8]. Other hypothesis is also associated with two different independent Sr sites. Dopant Eu^{2+} ion occupy two Sr sites. So the bond length between the Eu ion and its nearest oxygen neighbors is very important. And these bond lengths are different for Sr1 and Sr2 sites. The excitation band of the green emission could be related to the Sr1 site, the excitation band of the blue emission to the Sr2 site. We assume this hypothesis to be more plausible, because dopant Eu^{2+} ion causes redshift in the compound. And redshift arises as a result of the centroid shift and crystal field splitting. Dependence of these two quantities on the bond length between Eu ion and the nearest neighboring oxygen sites implies that they will also change in the Sr 1 and Sr2 sites. And it will be the main cause of blue emission band in emission spectrum at low temperatures [9].

We also made our experiments at lower temperature of about T=20K but at different exciting wavelength (λ=165nm, λ=206,6nm).

When we excited the sample with 165nm (7,5eV) different bands were observed there. The first peak (250nm) appears due to the intrinsic emission of aluminate matrix. The second one is observed at 380nm and corresponds to inter-band transitions. Band at 410 nm can be explained as the one above (figure 3) for 445 nm.

We can see that at 206,6nm exciting wavelength (6,1eV) these two bands are diminished. We only can see band at 445nm and Eu^{3+} ion line.

3.3 Afterglow properties of $SrAl_2O_4:Eu^{2+}$

The persistent luminescence lifetime can be enhanced by adding some trivalent Re^{3+} ions. But in this work we measured decay time of afterglow for $SrAl_2O_4$: Eu^2 (1%). There are a lot of models for explaining the afterglow process. But we believe that in our situation it can be explained by Aitasalo model. As described in this model the long persistent luminescence of $MAl_2O_4:Eu^{2+}$ might be caused by alkaline earth vacancies. It is known from the literature that this time should be in microseconds. In comparison the afterglow decay time in the literature is nearly 2 minutes.

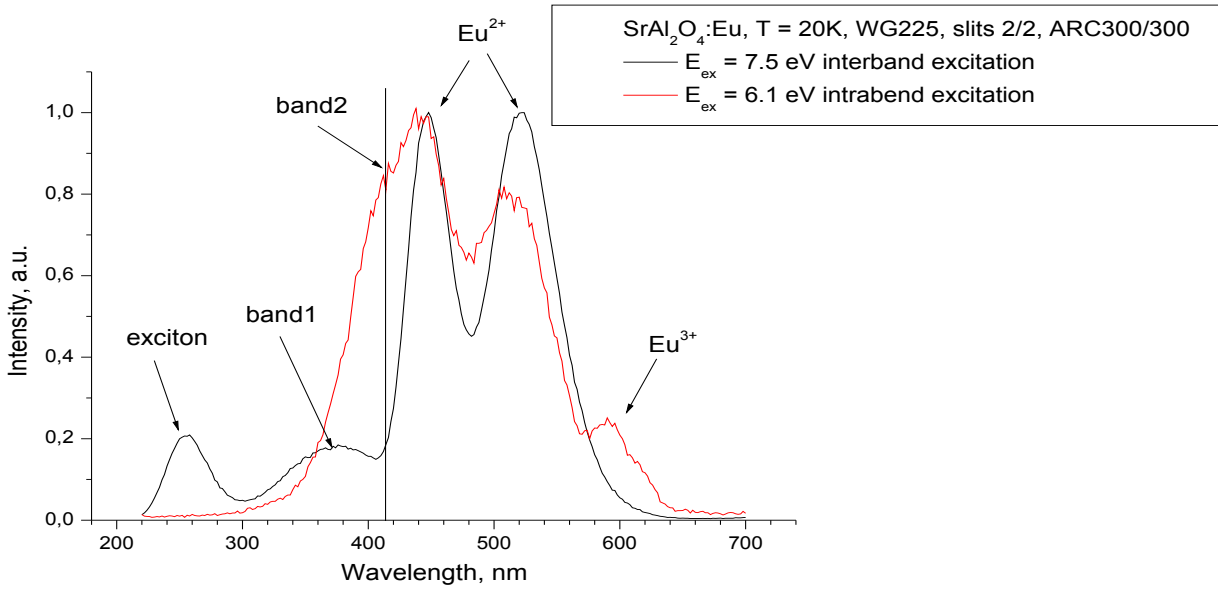

*Fig.5.*The excitation and emission spectra of $SrAl_2O_4$: Eu^{2+}at low temperature (20K) in different wavelengths.

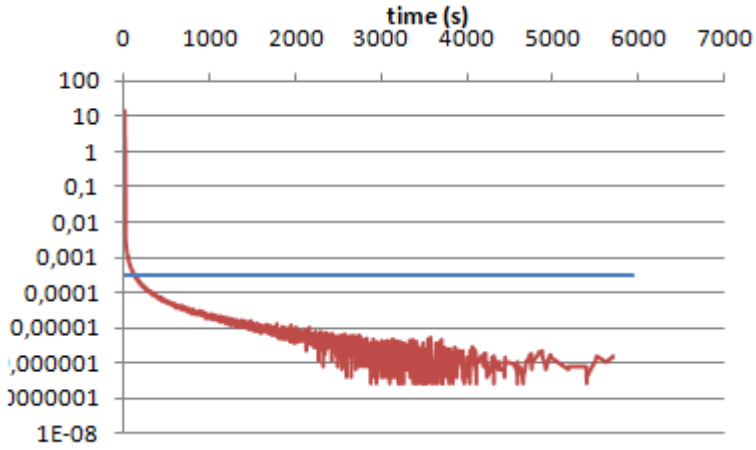

Fig. 6. Decay time of afterglow of $SrAl_2O_4$:Eu(1%).

CONCLUSION

We synthesized $SrAl_2O_4:Eu^{2+}$ by combustion method and measured PL properties at different temperatures. In contrast to the room temperature, at low temperatures (77, 150K) the second band arises. This material gives us 2 minute afterglow. It is a very interesting result because in most phosphors it is given in microseconds.

ACKNOWLEDGMENTS

The authors would like to express their sincere thanks to Dr. Rasim Jabbarov for scientific support.

[1] *Y. Zheng, D. Chen*. Luminescence, 26, 481 (2011).
[2] *S. Mammadova, H. Streit, T. Orucov, Ch.Sultanov.* Azerbaijan Journal of Physics .18, N4, 46 (2012).
[3] *T. Aitasalo, J. Hölsa, H. Junger , J.C. Krupa , M. Latusaari, J. Legendzieüicz, J. Niittykoski.* Radiation Measurements, 38, 727-730 (2004).
[4] *S. Calyn, M. Nazarov, A. Nor Nazida, and M. Ahmad –Fauzi* . Moldavian Journal of the Physical Sciences , 11,N1-2 (2012).
[5] *Xibin Yu, Chunlei Zhou, Xianghong He, ZifeiPeng, Shi-Ping Yang.* Materials Letters 58 1087 (2004).
[6] *F. Clabau, X. Rocquefelte, S. Jobic, P. Deniard, M.-H. Whangbo, A. Garcia, and T. Le Mercier,* Chem. Mater.**,** 17, 3904-3912(2005).
[7] *S.H.M.Poort, W.P.Blokpoel, and G. Blasse* . Chem. Mater .7,1547 (1995).
[8] *Jonas Botterman, Jonas J. Joos ,Phillipe F. Smet.* Physical Review B90 . 085147 (2014).
[9] *M. Nazarov, M.G. Brik , D. Spassky , B. Tsukerblat, A. Nor Nazida, M.N. Ahmad-Fauzi.* Journal of Alloys and Compounds, 573, 6–10 (2013).
[10] *T. Kobayashi, T. Sekine, N. Hirosaki.* Optical Materials 31**,** 886–888 (2009).
[11] *Jorma Hölsa, Högne Junger, Mika Lastusaari, Janne Niittykoski.* Journal of Alloys and Compounds, 323-324, 326 (2001).
[12] *Huayna Terraschke**,** Markus Suta, Matthias Adlung, Samira Mammadova, Nahida Musayeva, Rasim Jabbarov, Mihail Nazarov and Claudia Wickleder. unpublished.*
[13] *W. M. Yen, M. J. Weber.*CRC Press, (2004).

Recevied: 27.02.2015

THE INFLUENCE OF SAMARIUM IMPURITY ON MECHANISM OF CURRENT PASSING THROUGH Al-$Se_{95}Te_5$<Sm>-Te STRUCTURES

S.U. ATAYEVA, S.I. MEHDIYEVA, A.I. ISAYEV, V.Z. ZEYNALOV, G.M. DEMIROV
Institute of Physics of Azerbaijan NAS
Az 1143, Baku, G.Javid, 33
seva_atayeva@mail

It is established that current passing through Al-$Se_{95}Te_5$<Sm>-Te structures is carried out by monopolar injection mechanism at participation of traps for holes. The local level parameters (concentration and energy state) controlling the electric charge transfer are defined with the use of existing theories of injection currents. The obtained results are connected with distribution peculiarities of samarium atoms and their chemical activity.

Keywords: chalcogenide glass-like semiconductors, local levels, injection currents, charged centers.
PACS: 73.63

INTRODUCTION

The chalcogenide glass-like semiconductors (ChGS) are successfully applied in different devices of micro-, nano- and optoelectronics, i.e. in optic storage devices, planar waveguides, fiber amplifiers, optic switches, lasers and etc. [1-6]. Moreover, the given material field of application expands with time. The uniqueness of their electron properties in particular the transparency in visible and nearest IR regions, high photo-sensitivity, optical non-linearity, the ability to change such parameters as refractive index, optical-absorption edge and also potential possibilities of unlimited doping and technological process simplicity promotes to it. However, the application success requires the establishment of electron property controlling methods.

It is known in that ChGS materials the short-range order (SRO) in atom disposition similar to their crystal analogues saves but long-range order (LRO) destroys, i.e. the translation symmetry which is characteristic of crystals. Besides, there are heterogeneities of nano-meter dimension in them, i.e. the medium-range order (MRO) ranges in which there is a definite order in disposition of atoms and structural units. They play the essential role in electron property control similar to elementary cells in crystals. One can modify the dimensions and structures of MRO ranges and thus to influence on electron properties by change of technological process mode, chemical composition and also doping.

The charged centers D^+ and D^- with negative electron correlation energy (U^- are centers) also play the significant role in electron property control of chalcogenide glasses. The fact of paramagnetism absence, i.e. the absence of unpaired electrons, is the confirmation of their existence [7-8]. One can change the given center concentrations and thus directly change their electron properties by different methods. The present paper is devoted to the investigation of charged center role in transfer processes of electric charge through Te- $Se_{95}Te_5$ – Al structure and samarium impurity influence on it at accompaniment of injection from contacts. It is supposed that given centers create the local states in $Se_{95}Te_5$ forbidden band, the completing and ionization of which with field control the conduction mechanism in strong electric fields. The given composition choice in the capacity of investigation object is caused by the fact that the substitution of selenium atom parts by tellurium ones promotes to partial destroy of Se_8 rings, shortening of chain molecule length and dangling bound concentration increase. The use of samarium for doping connects with the fact that samarium as chemically active element revealing two- and three-valence and also taking part as positive ions, can form new structural elements with selenium and tellurium atoms and promote to change of relative concentration of charged centers. Thus, the use in capacity of addition of tellurium and samarium doping element should lead to change of structure and charged defect concentration of amorphous selenium that allows us to influence on its electron properties. This helps us to find the ways of successful practical use of given ChGS material, i.e. to broaden the region of its application.

THE EXPERIMENT TECHNIQUE AND SAMPLE PREPARATION

ChGS synthesis of $Se_{95}Te_5$ composition with samarium impurity is carried out by melting of corresponding qualities of essential purity chemical elements in vacuum quartz ampoules up to 10^{-4} millimeter of mercury at temperature 900 ^{0}C in rotating furnace with aftercooling in mode of switched furnace. The impurity is introduced in synthesis process, its concentration lies in limits 0,05÷1at %. The volt-ampere characteristics (VAC) are measured in stationary mode by standard technique. The samples are presented themselves “sandwich” with aluminum and tellurium electrodes and are prepared by the method of thermal evaporation in vacuum ~ 10^{-4} millimeter of mercury. The film thickness is measured by interferometric method and is varied in range 1-10μm. VAC of Al-$Se_{95}Te_5$<Sm>-Te structure is investigated at constant current at positive potential applied to Te.

EXPERIMENTAL RESULTS AND THEIR DISCUSSION

VAC of investigated structure at room temperature is shown on figure. As it is seen in double logarithmic scale VAC consists of several clearly marked straight-line portions corresponding to current power dependences (I)

on applied voltage (V). In many samples $I \sim V^n$ ($n \leq 1$) dependence is observed at small voltages. Further $I \sim V^n$ dependence where n takes the different values in VAC different portions that confirms the charge carrier transfer (holes) in given structure is carried out by monopolar injection current mechanism limited by volume charges (CLVC) at participation of charge capture traps [10]. As it is seen from graphs the samarium impurity has complex influence on current passing mechanism that one can explain by changes taking part in energy spectrum of localized states inside the forbidden band.

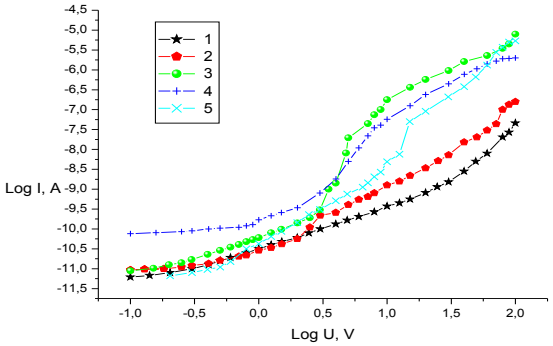

Fig. 1. The volt-ampere characteristics of $Se_{95}Te_5$ composition with samarium imprurity: 1is $Se_{95}Te_5$; 2is $Se_{95}Te_5Sm_{0,05}$; 3is $Se_{95}Te_5Sm_{0,1}$; 4is $Se_{95}Te_5Sm_{0,5}$; 5is $Se_{95}Te_5Sm_1$ taken at room temperature on films of thickness 3μm.

VAC of Al-$Se_{95}Te_5$-Te structure in initial portion satisfy to ohmic law which transit to the region corresponding to power law with voltage increase, i.e. $I \sim V^n$, where n exceeds 2. Such VAC behavior confirms that the electric charge transfer in given material is controlled by capture trap centers for holes situated higher Fermi level. Shallow levels (situated below Fermi level) either are absent, or the concentration of deep states so high one that their completing in given voltages isn't finished (big voltages lead to layer breakdowns). According to CLVC theory [10] the electric charge transfer is controlled by shallow levels after the fact that deep traps are fully completed by charge carriers. If one take into consideration that carrier transport [7-12] in ChGS materials is controlled by charged centers (D^+ и D^-) with high concentrations (for $Se_{95}Te_5$~ $10^{18}cm^{-3}$ [13]) then the prognosis confirm. In layers containing the small concentrations of samarium impurities (up to 0,1%), the voltage, at which the power dependence begins, shifts to the small voltage value and the quadratic dependence is observed in following region, i.e. $I \sim V^2$ which is substituted by power law with voltage increase again. This obviously is connected with decrease of deep trap concentration and formation of new shallow traps. VAC of layers with samarium impurity big concentrations (concentration ≥ 0,5at%) beginning from ohmic law transforms into quadratic one and region of trap total filing which is substituted by quadratic law with voltage increase. The power law of current strength dependence on applied voltage is observed in last portion. According to CLVC theory [10] such VAC behavior confirms the existence of two groups of shallow traps controlling the electric charge transfer.

The observable VAC changes of $Se_{95}Te_5$ layers with doping level change can be explained by peculiarities of samarium impurity atom distribution, their revealing in the form of positive ions in amorphous matrix and also by involvement of charged defect model. It is supposed that local electric fields existing round charged defects D^+ and D^- and structural distortions near them and also samarium big ion radius promote to the fact that D^- centers play role of ones effectively capturing samarium positive ions. Thus, samarium ions in small concentrations mainly accumulate round D^- centers in amorphous matrix that promotes to electric field screening of these centers. This leads to the fact that concentration of D^- defects, actively captured the holes decrease and that's why the region of trap limiting filling begins at small voltages and the shallow traps appear at not high voltages. It is supposed that in ChGS investigated system there are two groups of local states connected with selenium and tellurium atoms (as the shallow traps are observed in pure amorphous selenium). The new local states also situated below Fermi level form at big concentrations of samarium impurity.

Using the known theory of injection currents [10] in ChGS system of $Se_{95}Te_5$ doped by samarium one can define some parameters characterizing the electric charge transfer and also parameters of hole capture traps given in table 1.

From VAC ohmic portions the film resistivity values are calculated and using it, the concentrations of equilibrium free holes (table) are estimated according to formula $\rho = (ep_0\mu)^{-1}$ where e is elementary charge and μ is charge carrier drift mobility (for holes μ = 10^{-3} $cm^2/(V \cdot sec)$ [13]). Using these data Fermi level position in forbidden band ($F_o - E_v$), где N_v is effective state density in valence band ($N_v = 10^{20}$ $см^{-3}$ [7]), κT is heat energy, is defined by the following formula:

$$p_0 = N_v exp\left(-\frac{F_0 - E_v}{kT}\right) \qquad (1)$$

Table 1

	$Se_{95}Te_5$	$Se_{95}Te_5Sm_{0.05}$	$Se_{95}Te_5Sm_{0.1}$	$Se_{95}Te_5Sm_{0.5}$	$Se_{95}Te_5Sm_1$
ρ	$2.67*10^{12}$	$7.1*10^{12}$	$1.98*10^{12}$	$1.3*10^{12}$	$9.1*10^{12}$
P_0	$4.68*10^9$	$1.7*10^9$	$6.3*10^9$	$9.6*10^9$	$1.38*10^9$
F_0-E_v	0.62 eV	0.64 eV	0.61 eV	0.6 eV	0.65 eV
P_{t02}	$9.2*10^{14}$	$2.1*10^{14}$	$2.5*10^{15}$	$1.8*10^{14}$	$6.1*10^{14}$
E_{t2}-F_0	0.16 eV	0.2 eV	0.14 eV	-	-
P_1	-	$1.8*10^{15}$	$6*10^{15}$	-	$2.15*10^{15}$
E_{t1}-E_v	-	0.55 eV	0.51 eV	-	0.51 eV
E_{t2}-E_v	0.78 eV	0.75 eV	0.75 eV	0.58 eV	0.57 eV

The ohmic portion precedes to the one corresponding to fully completed trap for $Se_{95}Te_5$ samples without impurity and with small impurity content and that's why (p_{t02}) concentration primarily not taken by trap holes with E_{t2} energy is calculated from the following equation:

$$V_{FCT} = \frac{ep_{t02}L^2}{\varepsilon} \qquad (2)$$

and values are given in table. Here V_{FCT} is voltage at which the fully completed trap portion E_{t2} begins. As it is seen from table $p_{t02} \rangle\rangle p_0$. As it is above mentioned the deep levels are connected with D^- - centers in investigated materials. Taking the concentrations of (N_{t2}) given centers by 10^{18} cm^{-3} order [13] the energy position of level E_{t2} is calculated by the following formula:

$$p_{t02} = \frac{N_{t2}}{1 + g_A \exp(\frac{E_{t2} - F_0}{kT})} \approx \approx \frac{N_{t2}}{g_A} \exp(\frac{F_0 - E_{t2}}{kT}) \qquad (3)$$

It is considered that $g_A = 2$.

The quadratic dependence of current strength on voltage is observed in VAC portion following the region of fully completed deep traps, i.e. VAC satisfies to law:

$$I = \frac{\theta \varepsilon \mu V^2}{L^3} \qquad (4)$$

where θ characterizes the free carrier part of all injected ones.

$$\theta = \frac{N_c}{gN_t} \exp \frac{E_t - E_c}{kT} \qquad (5)$$

According to [7] only one discrete level influences on current. If there are several groups of shallow attachment levels that is expected in ChGS material containing the REE impurity atoms, then the group with θ least value more strongly restricts the current and parameter θ, connected especially with this group, includes into (4).

θ values are estimated by the following formula:

$$V_x \approx \frac{ep_0 L^2}{\theta L^2} \qquad (6)$$

where V_x is voltage at which $I \sim V^2$ dependence begins. Using the voltage at which the current strong increase is observed, the concentration of traps (p) are not occupied by holes is calculated by formula (2).

According to (10) in given case $p = N_{t1}$, where N_{t1} is total concentration of shallow traps. Knowing N_{t1} and θ, the accumulation depths of the given traps the results of which are shown in table, are calculated by formula (5).

The quadratic dependence of current strength on voltage precedes the VAC portion corresponding to current strength strong increase for $Se_{95}Te_5$ samples with samarium big concentrations (0,5; 1 at%), that confirms the fact that traps controlling the charge transport are shallow ones, i.e. they posit below Fermi level.

Using (2), (5) and (6) formulae, the concentration and accumulation depth of traps for these samples are defined and obtained results are given in table.

CONCLUSION

It is established that current passing through Al-$Se_{95}Te_5$<Sm>-Te structures is carried out by monopolar injection mechanism at participation of traps for holes. It is shown that doping by samarium strongly influences on current passing mechanism in investigated structure that is explained by change taking place in energy spectrum of local states. In pure $Se_{95}Te_5$ electric charge transfer is controlled by homoenergetic levels posited higher Fermi level. In $Se_{95}Te_5$ containing the small concentrations of samarium impurity (0,1 at %) the current passing mechanism is controlled by two groups of local levels posited on both sides of Fermi level.

In $Se_{95}Te_5$ doped by samarium high concentrations (0,5; 1 at %) the two groups of local levels posied below Fermi level (both levels are shallow ones) take part in controlling of current passing. It is supposed that local levels are connected with dangling bonds: deep levels are connected with tellurium atoms (D^- is center), shallow ones are connected with selenium atoms. The local level parameters (concentration and energy positions) are defined by use of existing theories of injection currents. The obtained results are connected with distribution peculiarities of samarium atoms and their chemical activity.

[1] *I. Aggarwal and J. Sanghera*. Development and applications of chalcogenide glass optical fibers at NRL// Optoelectron.Adv.Mater. **4**(3),(2002),c.665-678.

[2] *J. Viens, C. Meneghini, A. Villeneuve, T. Galstian, E. Knystautas, M. Duguay, K. Ricardson, and T. Cardinal.*Fabrication and characterization of integrated optical waveguides in sulfide chalcogenide glasses// J. Lightwave Technol. **17**(7),(1999),c.1184-1191.

[3] *Y. Ruan, W. Li., R. Jarvis, N. Madsen, A. Rode, and B. Luther-Davies.* Fabrication and characterization of low loss rib chalcogenide waveguides made by dry elching// Opt. Express. **12,** (2004), 5140-5145.

[4] *A. Zakery and S. Elliott.* Optical properties and applications of chalcogenide glasses, J. Non-Cryst., **330** (2003) 1-12.

[5] *S.G. Bishop, D.A. Tumbull, B.G. Aitken.* Excitation of rare earth emission in chalcogenide glasses by

broadband Urbach edge absorption., J. Non- Cryst Solids, **266-269** (2000)876-883.

[6] *T. Carrig,* Transition-metal-doped chalcogenide lasers// J.Electron. Mater.,**31**, (2002), 759-769.

[7] *N.F. Mott, E.A. Devis.* (M., Mir, 1982). [Per.s. anql.:N.Mott, E. Davis, Electronic processes in non-cryst. solids] 662s. (In Russian).

[8] *K.D. Chendin.* Elektronnie yavleniya v xalkoqenidnix stekloobraznix poluprovodnikov. Sankt-Peterburq, Nauka(1996) 486s. (In Russian).

[9] *A.I. Isayev, S.I. Mekhtieva, N.Z. Jalilov, R.I. Alekperov, G.K. Akberov.* Localised states in the band gap of chalcogenide glass-like semiconductors of Se-As system with Sm impurity// Solid State Communications, **149**, ISS 1-2, (2009), p. 45-48.

[10] *M. Lampert, P.Mark.* Injeekchionnie toki v tverdix telax. (M., Mir, 1976) 416 s. (In Russian).

[11] *L.P. Kazakova, E.A. Lebedev, A.I. Isaev, S.I. Mekhtieva, N.B. Zakharova, I.I. Yatlinko.* FTP, **27**(6), (1993), 959-965. (In Russian).

[12] *L.P. Kazakova , E.A. Lebedev, N.B. Zakharova, I.I. Yatlinko, A.I. Isayev, S.I. Mekhtiyeva.* S., Improvement of charge transport in Se-As glasses by doping with halogens// *J. of* Non Cristalline solids, **167**, (1994), 65-69.

[13] *S.I. Mekhtieva,* A.*I. Isayev, E.A. Mamedov.* Sbornik trudov III Mejdunarodnoy konfer. Amorfnie i mikrokristallicheskie poluprovodniki, Sankt-Peterburq (2002) s. 204. (In Russian).

Recevied:05.12.2014

THE DEPENDENCE OF DIELECTRIC PARAMETERS AND ELECTRIC CONDUCTION OF COMPOSITE ON THE BASE OF POLYETHYLENE AND IRON OXIDE ON RADIATION DOSE

N.Sh. ALIYEV, A.M. MAGERRAMOV, M.M. GULIYEV, R.S. ISMAYILOVA
Insitute of Radiation Problems of Azerbaijan NAS
Az1043, Baku,B.Vahabzade str.,9
nabi.aliyev.1958@mail.ru

The radiation γ-influence at 0-500kGy doses on dielectric parameters (ε' and tgδ) and composite electric conduction (ζ) on the base of high-density polyethylene (HDPE) and iron oxide (α-Fe_2O_3) radiated in air at room temperature is studied with the aim of modification of new class composite properties polymer –metal oxide. It is shown that ε'=f(D) and tgδ=f(D) dependences have extreme character at(10 and 20 %) α-Fe_2O_3 high concentrations. ζ=f(D) dependence of investigated samples also has extreme character (besides composite HDPE+20%α-Fe_2O_3) and it is explained by accumulation of stabilized charge carriers in them.

Keywords: HDPE/α-Fe_2O_3, γ-radiation dose, dielectric constants, dielectric losses, electric conduction.
PACS: 71.38

INTRODUCTION

The modern state of development of cosmic, atomic and electronic industries requires the creation of new polymer materials and composites on their base for usage of multifunctional electron devices in the capacity of electro-active elements. In exploitation process these materials are subjected to influence of different external factors (mechanical load, thermal field, corrosive medium, humidity, ionizing radiation and etc), as a result of which their properties and structure change. In particular, the polymer composite materials (PCM) are successfully applied in the capacity of anti-damage nuclear reactor shielding, in power-supply system of artificial satellites and spaceships where there is always the nuclear radiation. The radiation-induced behavior of PCM properties is the important aspect, which should be taken into consideration at development of new PCM working in conditions of nuclear radiation. That's why new PCM should have high radiation resistance and minimal dependence of properties on change of environment parameter [1-4].

It is well known [5-6] that intermolecular linkage or destruction (chain breakage) of polymers at γ-radiation and this fact that which of these processes dominate depends on chemical structure, stability of formed free radicals and polymer aggregate state. The study of γ-radiation influence on PCM in particular, on their electrophysical properties still is of interest for many scientists and is important not only for fundamental investigation and for study of radiation process mechanism in these materials. The influence of γ-radiation is the topic of the many investigations [7-10].

The experimental investigation of γ-radiation influence on electrophysical properties of composite system HDPE/ α-Fe_2O_3 is the aim of the present paper.

EXPERIMENTAL PART

The powder-like high-density polyethylene by 20806-024 mark with average molecular mass 95000, crystallinity degree 52%, melting point 130˚C and density 958kg/m^3 is chosen in the capacity of dielectric (matrix). HDPE choice as matrix is caused mainly by well dielectric properties of material and its manufacturability.

For the obtaining of samples of unfulfilled HDPE and HDPE+α-Fe_2O_3 composites the following technological scheme is applied:

- the obtaining by way of sifting of α-Fe_2O_3 powders with particle dimensions not more 30μm;
- the drying during 24h. at T =100˚C and mixing in porcelain mortar of powder-like α-Fe_2O_3 with HDPE powder;
- the pressing of homogeneous mixture of component powders in hydraulic press with incalescent plates at pressure 15MPa with endurance at temperature 150˚C during 5min and obtaining of composite samples in the form of discs by diameter 20mm and thickness 140÷180μm. All concentrations given in the present paper are volume ones;
- the pressing of electrodes on both surfaces of samples from thin aluminum foil 7μm with further cooling in water-ice mixture (quenching mode) with aim of supply of reliable electric contact between sample and electrodes from stainless steel. All composites are subjected to temperature stabilization at 60˚C during 24h after which all samples are considered as suitable for investigations.

The previous radiation of samples by γ-rays are carried out in air on γ-source Co^{60} with dose rate D=3,3·10^3 Gy/h up to 500κGy. The dose rate in radiation point is defined with the help of ferro-sulfate dosimeter.

The investigations of dielectric characteristics (of real part of ε dielectric constant and tgδ dielectric loss tangent) are carried out by two-electrode system at 10^3Hz frequency, at 20˚C temperature and U=1V measuring voltage amplitude with application of specially screened and earthed heated measuring cell by "sandwich" type having the system of measuring and potential electrodes by diameters 10 and 15mm correspondingly. The samples are put into measuring cell with clamping electrodes from stainless steel. The sample temperature is controlled with the help of thermocouple cuprum-constantan. The measuring of C capacity and tgδ of samples are carried out with the help of wideband precision immittance measurer of E7-20 type and

measuring of R volume resistance with help of E6-13A teraohmmeter. Further, ε' value ($\varepsilon'=c\cdot d/\varepsilon_0\cdot S$, where S is plane sample square, d is film thickness) and electric conduction value ζ ($\zeta = d/R\cdot S$, where R(Ом) is sample resistance) of measuring cell with sample is defined on base of measured values of given parameters and sample geometric dimensions by standard methods.

RESULTS AND THEIR DISCUSSION

The changes of real component of complex dielectric constant ε' of HDPE and composites with filler concentrations α-Fe_2O_3 up to 20 % before and after influence of γ-radiation are shown on fig.1. From the figure it is seen that ε' increases from 2,3 for HDPE up to 3,8 for HDPE+20% α-Fe_2O_3 composite with α-Fe_2O_3 concentration increase and it slowly increases with absorption dose increase. ε' firstly insignificantly increases for samples with volume contents 10 and 20 % α - Fe_2O_3, achieves maximum at dose D=300kGy and further decreases. ε' value in maximum is 4,8, i.e. it increases approximately in 1,26 times (≈26%), in given region of exposure radiation dose for HDPE+20%α-Fe_2O_3 composite. Such character of ε' dependence on absorbed radiation dose is explained by formation of end and intra-chain peroxide radicals and their destruction by reaction:

$$R^{\cdot} + O_2 \rightleftarrows RO^{\cdot}_2$$

By other hand [11], the material crystallinity degree decreases with the increase of absorbed radiation dose, crystal structure gradually destroys and totally disappears at high doses. Especially this process of crystal structure disorder and also the increase of dipole element number (C=0 group, dipole moment $9{,}35\cdot10^{-30}$ C·m) leading to ε' increase are main factors defining the change of HDPE polymer matrix properties and composites as a whole on its base. It is necessary to note that dipole element number increase leading to formation of wide series of polar elements appearing on boundary particle-polymer matrix takes place at composite obtaining too (as a result of partial matrix oxidation and stabilization of α - Fe_2O_3 particles in it). The results of dielectric loss tangent change of investigated samples are given on fig.2. It is seen that introduction of α-Fe_2O_3 up to 20% into HDPE leads to dielectric loss increase from 0,008 up to 0,1 with respect to pure HDPE. From the figure it is also seen that tgδ composite values in given region of absorption dose increase with D increase, pass through the maximum at 300 and 100kGy and later decrease. tgδ increase observed in initial period is connected with increase of oxide groups (formed mainly because of solved oxygen), unsaturation and amorphism degree of polyethylene matrix. In HDPE+5%α-Fe_2O_3 case tgδ with D increase insignificantly decreasing achieves the minimum at 100kGy in interval (100÷300)кGy practically remains constant and further also insignificantly increases. For pure HDPE tgδ value with D increase practically doesn't change up to absorbed dose 500kGy. The typical curve of function ζ = f(D) are shown on fig.3. ζ value extreme change with radiation dose is observed practically in all cases. The electric conduction on constant current of sample composites with 5 and 10% volume content of filler α-Fe_2O_3 correspondingly is subjected to the biggest change.

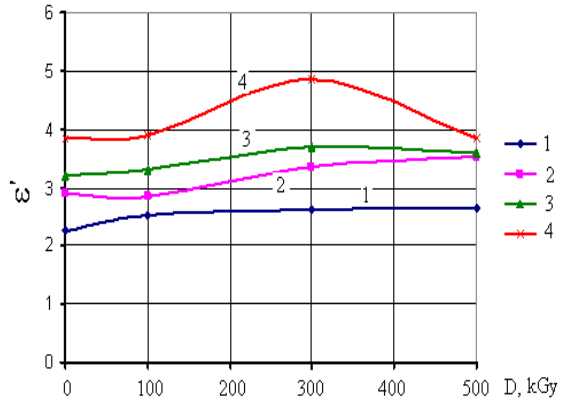

Fig.1. The dependences of dielectric constant (ε′) on HDPE+αFe_2O_3 composite radiation dose: 1 is pure HDPE, 2 is HDPE+5%α-Fe_2O_3 ,3 is HDPE+10% α-Fe_2O_3, 4 is HDPE+20% α-Fe_2O_3.

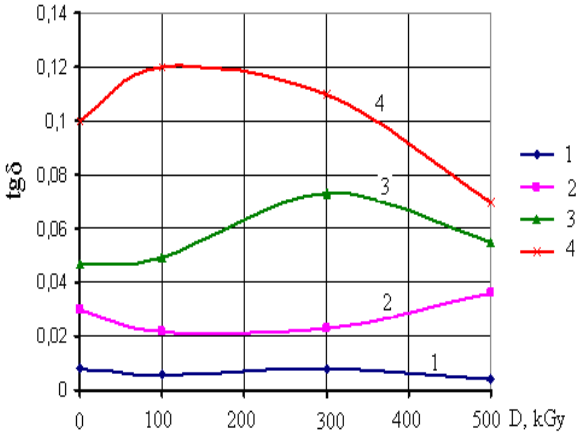

Fig.2. The dependences of dielectric loss (tgδ) on HDPE+αFe_2O_3 composite radiation dose: 1 is pure HDPE, 2 is HDPE+5%α-Fe_2O_3 ,3 is HDPE+10% α-Fe_2O_3, 4 is HDPE+20% α-Fe_2O_3.

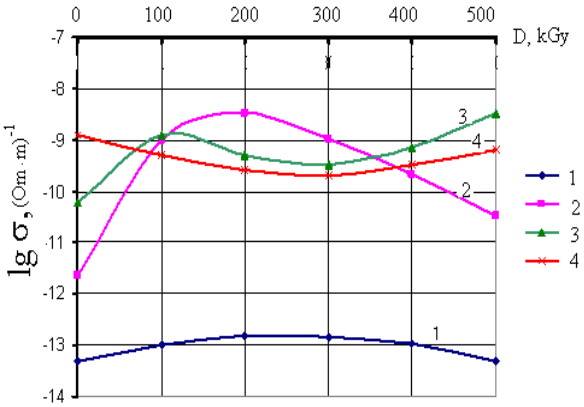

Fig.3. The electric conduction dependences (σ) on HDPE+αFe_2O_3 composite radiation dose: 1 is pure HDPE, 2 is HDPE+5%α-Fe_2O_3 ,3 is HDPE+10% α-Fe_2O_3, 4 is HDPE+20% α-Fe_2O_3.

The electric conduction of these samples with D increase achieves the maximum at D=200 and D=100kGy correspondingly. The further increase of absorption dose leads to ζ decrease of HDPE+5% α-Fe_2O_3 composites and in case of HDPE+10%α-Fe_2O_3 composite the electric conduction decreasing achieves minimum at 300kGy and later increases again. The electric conduction of pure HDPE and HDPE+20% α-Fe_2O_3 composites in given dose interval practically remains constant. It is seen that HDPE filling up to 20%α-Fe_2O_3 leads to electric conduction increase from $4{,}44\cdot10^{-14}$ $(Om\cdot m)^{-1}$ up to $3{,}5\cdot10^{-10}(Om\cdot m)^{-1}$. Note that as a whole the absorbed dose weakly influences on dose dependences of investigated samples (besides HDPE+5%α-Fe_2O_3). One can suppose that some increase of electric conduction observing at γ-radiation is caused by ionization. The ionization produces the charges able to motion (free electrons and positive ions) which can take part into conduction process. In [12] it is seen that at γ-radiation of HDPE the accumulation of volume electric charge correlates with formation and accumulation of peroxide radicals, which are electron acceptors and define the whole process of charge accumulation. By authors' opinion [13] the dose effects are the direct consequence of free radical formation and their recombination between each other with formation of character postradiational changes in polymer structure. Moreover, the some ovservable increase of electric conduction of investigated samples one can connect with linkage processes of polymer chains leading to three-dimensional structure formation and further its decrease one can connect with oxide destruction processes.

The authors [14] confirm that electric conduction of polyethylene matrix is caused by charge carriers which appear at γ-radiation and not by charges injected from electrodes. The concentration of trapped electrons increases with radiation dose increase: the more radiation doses the bigger number of charge carriers.

The radiation dose increase leads to decrease of relation of crystal phase to amorphous one and by this it causes the decrease of phase interface square. As a result of this the concentration density of deep traps on phase interface increases.

Thus, the dose effects, i.e. the influence of absorbed dose of γ-radiation on electro-physical properties of previous radiation is caused not by spectrum change of molecular motions, but accumulation in radiated material of stabilized charge carriers and less radical or molecular radiolysis products which act as trap centers.

[1] *L. Boudou, J. Gustavino*. Influence of temperature on low-density polyethylene films through conduction measurement. J. PhysD: Appl.Phys.2002, 35:1555-1561.

[2] *A.Bhattacharya.* Radiation and industrial polymer. Prog. Polym. Sci. 2000, 25: 371-401.

[3] *D. Kostoski, J. Dojcilovic, L. Novakovic, E. Suljovrujic.* Effects of charge trapping inf gamma irradiated and accelerated aged low-density polyethylene. Polym. Degrad. Stab., 2005, 91:2229-2232.

[4] *M. Borhani, G. Mirjalili, F. Ziaie, M.A. Bolrizadeh.* Electrical properties of EVA/LDPE blends irradiated by high energy electron beam. Nucleonika 2007; 52 (2): 77-81.

[5] *H. Kashiwabara, S. Shimada, Y.Hori.* Free radicals and crosslinking in irradiated polyethylene. Radiat. Phys.Chem. 1991, V.37, №1, PP.43-46.

[6] *S.R. Allayarov, L.D. Kispert, V.Q. Nikolskiy, D.P. Kiryukin, D.A. Qordon, A.I. Mixaylov, D.A. Diksen.* Plasticheskie massi, 2009, №2, s.20-27. (In Russian).

[7] *D.N. Sadovnichiy, A.P. Tyutnev, Yu.M. Milekin, S.A. Xatipov.* Ximiya visokix enerqii. 2003, t.37, №6, s 436-441. (In Russian).

[8] *A.M. Maqerramov.* Strukturnoe I radichionnoe modifichirovanie elektretnix, pezoelektricheskix svoystv polimernix kompozitov. Baku-Elm, 2001, 327 s. (In Russian).

[9] *M.M. Kuliyev.* Study pf Polymer-Pieroceramic Composites by the Radio-Thermoluminescence Method. Surface Engineering and Applied Electrochemistry, 2007, v.43, №6, pp.508-511.

[10] *A.M. Maqerramov, M.M. Kuliyev, R.S. Ismayilova, E.Q. Qadjieva.* Tezisi 9-oy mejd. konf. "Yadernaya i radiachionnaya fizika", 24-27 sentyabr 2013, Almati, Kazaxstan. (In Russian).

[11] *A.V. Vannikov, V.K. Matveev, V.P. Sichkar, A.P. Tyutnev.* Elektricheskie svoystva. Izd-vo "Nauka", M. 1982, 272 s. (In Russian).

[12] *V.V. Qromov.* JFX, 2005, t.79, №1. s.121-125. (In Russian).

[13] *A.P. Tyutnev, V.S. Saenko, I.A. Smirnov, E.V. Pojidaev.* Ximiya visokix enerqiey, 2006, t.40, №5, s.364-375. (In Russian).

[14] *G. Chen, R.A. Fouracre, H.M. Banford, D.J. Tedford.* The effects of gamma-irradiation on thermally stimulated discharge current spectra in low-density polyethylene. Radiat. Phys. Chem. 1991, v.37, №3, pp.523-530.

Recevied:03.10.2014

SURFACE PHONONS IN TWO-LAYER THIN FILMS OF GeSe

F.M. HASHIMZADE, D.A. HUSEINOVA, Z.A. JAHANGIRLI, B.H. MEHDIYEV
Institute of Physics, National Academy of Sciences of Azerbaijan,
AZ 1143, Baku, Azerbaijan

This paper presents ab inition calculations of the surface phonon spectra of GeSe layered semiconductor compound, based on the Density Functional Perturbation Theory (DFPT). The surface has been imitated by a structure of periodically arranged slabs of two layers of GeSe crystal separated from other identical layers by the layers of vacuum sufficiently wide to ignore the effect of the upper boundary of the double-layer upon its lower boundary. We discuss the character of the surface modes located in the gaps, in the pockets, and in the area of allowed phonon states for the bulk GeSe crystals, as well as outside (above and below) the boundaries of the bulk phonon states.

Keywords: Density-functional theory, semiconductor surfaces, surface structure, surface dynamics.
PACS: 61.50.Ah, 62.50.-p, 64.70.kg, 71.15.Nc, 71.20.Nr.

1. INTRODUCTION

GeSe layered compound (along with *GeS*, *SnSe* and *SnS*) with strongly pronounced anisotropy of physical properties has interesting electronic, optical and dynamic properties. These compounds are promising materials for manufacturing of photodetectors and lasers in the near-infrared range, and are used as the cutoff devices and as the absorber materials in the non-toxic photovoltaic devices. Despite the fact that the electronic and optical properties of these compounds are well studied, the dynamic properties, particularly the dynamic surface properties, have remained virtually unexplored.

It is well known that various lattice defects and surface effects change electronic spectrum of a crystal. The presence of impurities and surface effects also drastically change the vibrational spectrum of a crystal. The existence of a surface can lead to the appearance of local and resonant states that are not present in a perfect crystal. Local and resonant states always affect the structure and the optical phonon spectra in semiconductors. Since real crystals contain the surface the effect of which cannot always be neglected, proper consideration of the effect of defects is essential in the analysis and interpretation of experimental data,. Furthermore, surface and interface structure are currently important working elements in many semiconductor devices.

The linear response formalism is known to yield reliable results for the lattice dynamics of both bulk and surfaces of a large variety of covalent crystals [1]. It has been shown that the density functional perturbation theory (DFPT) can be successfully applied to layered systems, such as *GeSe*, where the interlayer bonding is governed by van der Waals-type forces [2]. In this paper we present an ab initio calculation of the germanium selenide surface phonon structure based on DFPT.

2. THE CRYSTAL STRUCTURE AND CALCULATION METHOD

GeSe has an orthorhombic structure and belongs to the P_{nma} (D_{2h}^{16}) space group. Its lattice parameters are a=4.414 Å, b=3.862 Å and c=10.862 Å. The positions of the atoms in the structure, in fractional coordinates, are as the following : both atoms are at 4c as $\pm(x;1/4;z)$ and $\pm(1/2-x;3/4;1/2+z)$ [3]. A unit cell contains eight atoms organized in two adjacent double layers that are perpendicular to the direction of the c-axis. The atoms in each double layer bond to their three nearest neighbours by covalent bonds and form a zigzag chain along the direction of the minor axis of the crystal. As a consequence of the dominant van der Waals character of the bonds between adjacent layers, this material cleaves easily along the [001] planes.

All commonly used approaches to calculation of the frequencies of surface phonons are based on the slab method. Here we use the geometry of the periodically arranged slabs, wherein each slab comprises two layers. Adjacent slabs are separated by vacuum with the thickness of 13.72 Å. The thickness of each layer, which in turn consists of four atomic planes arranged in sequence Ge-Se-Se-Ge, equals 2.585 Å and the interlayer distance is 2.691 Å. Thus, the overall thickness of the GeSe slab is 7.86 Å. The model that we constructure for this superstructure also contains 8 atoms in a unit cell, but its symmetry is significantly lower, namely, the P21/m (No.11) space group. The calculations were performed in the DFPT framework based on the plane-wave pseudopotential method and implemented in the ABINIT program package [4].

The exchange-correlation interaction has been described in the local density approximation scheme [5]. For the norm-conserving pseudopotentials we used the Hartvigsen-Goedekker-Hutter (HGH) pseudopotentials [6]. In the expansion of the wave functions we included the plane waves with energies up to 40 Ha, which ensures a good convergence of the total energy. The equilibrium structure has been determined by minimizing the total energy relative to the lattice parameters, and the internal structure parameters have been optimized using Hellmann-Feynman forces . The minimization process was carried out until the force modules become less than 10-7 Ha/Bohr. The integration over the Brillouin Zone (BZ) has been carried out by $4\times4\times1$ partition shifted from the origin by (0.5,0.5,0.5), according to the Monkhorsta-Pak

scheme [7]. We use the ANADDB routine from the ABINIT package for the Fourier transforms to construct the dispersion law of the phonon modes over the entire BZ; this allows calculating phonon frequencies in arbitrary points of the BZ. In the calculated density of the phonon states one can see the resonances, the anti-resonances, and the gap and localized states.

3. DISCUSSION OF THE RESULTS

In addition to the localized surface states and the resonant surface zones, the phonon-dispersion curves of a crystal with surface contains the bulk zones. The latter correspond to the eigenstates that are delocalized in the direction perpendicular to the surface, and their energies correspond to the energies of states in an infinite bulk crystal. To determine the phonon spectrum of a crystal with surface one has to project the zones of a bulk crystal onto the first surface BZ.

The calculated projected bulk dispersion curves, the surface modes and the mixed modes along symmetrical directions of the BZ for GeSe are shown in Fig. 1. In the projected zone structure one can see energy gaps and energy pockets where the localized states are located.

An important feature of the spectrum of the surface phonon states is the appearance of high-frequency surface modes above the optical continuum at point **Γ**. Since the surface atoms have fewer nearest neighbours for bonding, the restoring forces and, consequently, the force constants on the surface are smaller than in the bulk. Therefore, one should expect that the surface modes will have lower frequencies compared to the bulk modes. In our case the surface phonons have higher frequencies than the bulk ones. This can be explained by the fact that in GeSe on (001)-surface during the relaxation of the surface atoms the bonds between the surface atoms change, and, as a result, the effective force constant increase. Indeed, the results of the calculations of atomic relaxations show that near the border with vacuum the lengths of the "vertical" *Ge-Se* bonds (2.48 Å) are sigificanlty shorter than the bond length in the bulk (2.51 Å) whereas the "horizontal" bonds almost do not change (2.58 Å). Therefore, the surface phonon modes appear above the optical bulk continuum as shown in Fig. 1.

The topmost mode does not mix with bulk states and can be observed as true surface vibrations throughout the two-dimensional BZ. The lowest surface mode which starts at point **Γ**, as a shear-horizontal mode, is the Rayleigh wave (RW).

In addition, one can identify a group of surface states in the forbidden zone between two zones that are fully localized at the surface. All other surface states fall in the area of the bulk vibrations and can be classed as mixed states, when both the bulk and the surface atoms participate in vibrations.

Fig. 1 also shows the local density of states (LDOS), along with the bulk density. One can identify two regions in the LDOS for the surface layer. The main contribution into the first peak in the first area comes from the low-frequency modes located below the bulk states. The first and the last peaks in the second region are determined by the vibrations in the forbidden gap, and these have the localized character of vibrations. All other peaks are mixed vibrations. This indicates strong hybridization of the vibrational states of the surface and of the bulk.

4. CONCLUSION

In this paper we present the results of ab initio calculations of the phonon dynamics of the GeSe (001) surfaces. We demonstrate that the localized modes appear in the gaps of the bulk continuum as well as within the pockets of the bulk subbands for certain directions of symmetry. The projected phonon dispersion curves revealed the presence of a Rayleigh mode. A change in the surface force constants signifcantly modifies the qualitative features of the surface phonon spectra.

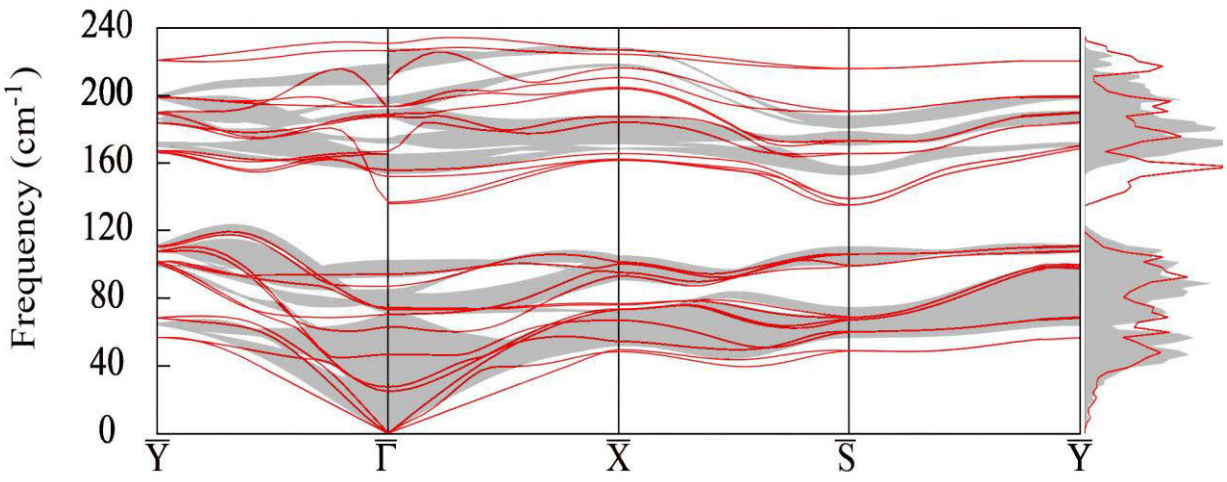

Fig 1. Calculated phonon spectra and phonon density of states (inset to the right side) of GeSe.

[1] *J. Fritsch, U. Schroder*. Physics Reports, 1999, **309**, 209.

[2] *V. Panella, A. L. Glebov, J.P. Toennies, C. Sebenne, C. Eckl, C. Adler, P. Pavone, U. Schroder*. Phys. Rev. B, 1999, **59** , 15772.

[3] *H.C. Hsueh, H. Vass, S.J. Clark, G.J. Ackland, J. Crain.* Phys.Rev. B, 1995, **51**, 16750.

[4] *X. Gonze, J.M. Beuken, R. Caracas, F. Detraux, M. Fuchs, M. Rignanese, L. Sindic, M. Verstraete, G. Zerah, F. Jallet*. Comput. Mater. Sci., 2002, **25**, 478.

[5] *S. Goedecker, M. Teter, J. Huetter*. Phys. Rev. B, 1996, **54**, 1703.

[6] *C. Hartwigsen, S. Goedecker, J. Hutter*. Phys. Rev. B, 1998, **58**, 3641.

[7] *H. Monkhorst, J. Pack.* Phys. Rev. B,1976, **13**, 5188.

Recevied:07.01.2015

DETECTION OF TERNARY FISSION FRAGMENTS FROM ^{252}CF WITH A POSITION-SENSITIVE ΔE-E TELESCOPE

G.S. AHMADOV*[1,2,4], F.I. AHMADOV[2,4], Yu.N. KOPATCH[1], S.A. TELEZHNIKOV[1], C. GRANJA [3], A.A. GARIBOV[2,4], S. POSPISIL[3]

Joint Institute for Nuclear Research, Dubna, Russia[1]

Institute of Radiation Problems-ANAS, Baku, Azerbaijan[2]

Institute of Experimental and Applied Physics, Czech Technical University in Prague, Czech Republic[3]

National Nuclear Research Centre of Ministry of Communications and High Technologies, Baku, Azerbaijan[4]

**email:ahmadovgadir@gmail.com*

Using a thin silicon diode detector with thickness of 12 μm coupled with a Timepix detector (equipped with a 300 μm silicon sensor), a position-sensitive ΔE-E telescope has been constructed. The telescope provides information about position, energy, time and type of registered particles. The emission probabilities and the energy distributions of ternary particles (He, Li, Be) from ^{252}Cf spontaneous fission source were determined using a pair of these telescopes operated in coincidence and with synchronized readout. The response of Timepix detector to different particle species was tested by ternary particles.

Keywords: Ternary fission, ΔE-E method, Timepix pixel detector, PIN diode.
PACS: 25.85.Ca, 29.40.Gx, 29.40.Wk.

INTRODUCTION

Normally, fission is a binary process, in which the fissioning nucleus splits into two fission fragments. This is the case in general for both spontaneous and induced nuclear fission. Sometimes, however, instead of the standard "binary fission" a higher-multiplicity process with three or more charged particles emitted in the outgoing channels is observed. The accompanying particles are lighter compared to the main binary fragments. Therefore, they are called light charge particles (LCP). In ternary fission process, mostly H and He isotopes are emitted, although particles up to mass 36 have been observed [1, 2, 3]. Ternary fission process for different nuclei has already been extensively investigated with various detectors and methods. About 87% of ternary fission events are the ternary ^{4}He particles with mean energy around 16 MeV. These are often called Long Range Alpha (LRA) particles [4, 5].

1. A ΔE-E TELESCOPE

Each side of the de-e telescope consists of 12 μm thin silicon and 300 μm Timepix pixelated detector. The thin silicon detector is used for ΔE measurement and the Timepix detector for E measurement. A simplified electronic scheme of the set-up is presented in Fig. 1. All signals from the ΔE detector are first pre-amplified. Signals from a charge-sensitive preamplifier are split in two parts. One part of the signal is fed to a spectroscopic amplifier for energy measurements and the second to a fast timing filter amplifier, then to constant fraction discriminator for triggering the Timepix detector (E). A 250 MHz DT5720 CAEN digitizer is used for pulse height spectrum measurements for the ΔE detector [6]. Each telescope was placed at a distance of 8 mm from the source.

Main part of the telescope is the hybrid pixel detector Timepix. It is used as E detector. Timepix is equipped with a single discriminator per pixel and works either as a hit counter, as a timer relative to the detection of the particle, or as a time over threshold counter. In summary, each Timepix pixel is equipped with a counter operating in one of the three modes: Medipix mode (the counter counts incoming particles), Timepix mode (the counter works as a timer and measures time of the particle detection) and Time over threshold (TOT) mode. In this last mode of operation, the Timepix is analogous to a Wilkinson type ADC, allowing direct energy measurement in each pixel. From its time over threshold (TOT) mode of operation, the Timepix device can count the amount of charge being deposited by a particle in a given pixel element. Timepix consists of 256 x 256 square pixels with pitch of 55 μm [7]. The total energy of the particle is measured by summing over all pixels in the cluster of activated pixels. The measured charge distributions can be fitted to a Gaussian shape, permitting the determination of the point of interaction of the particle in the device with sub-pixel precision.Its spatial resolution can be achieved down to few μm [8]. Timepix detector is controlled with the special readout interface FITPix and plugged to PC via USB [9]. The interface can be controlled via Pixelman software [10].

2. MEASUREMENT

For the measurements it is used a thin (both sides) spontaneous fission source of ^{252}Cf with activity of about 100 Bq mounted on a 60 μg/cm^2 foil backing of Al_2O_3 and coated with a thin layer of gold (of less than 10 mg/cm^2). The source thickness is assumed to be uniform to within 20%. The source was round with outer diameter 18 mm and inner diameter 2.1 mm. The experiment was carried out in vacuum (<0.4 mbar) with two telescopes oppositely placed at 8 mm from the source. The count rate for ternary fission was 0.3/min on each telescope.

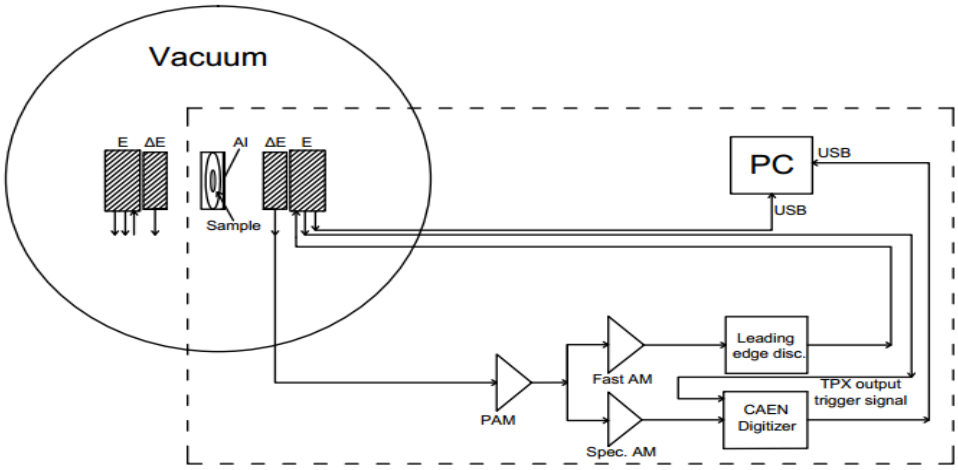

Fig.1. Schematic presentation of the detector configuration. One side of the set-up has a thin ΔE-detector (12 μm) and the hybrid pixel detector Timepix as E detector (300 μm).

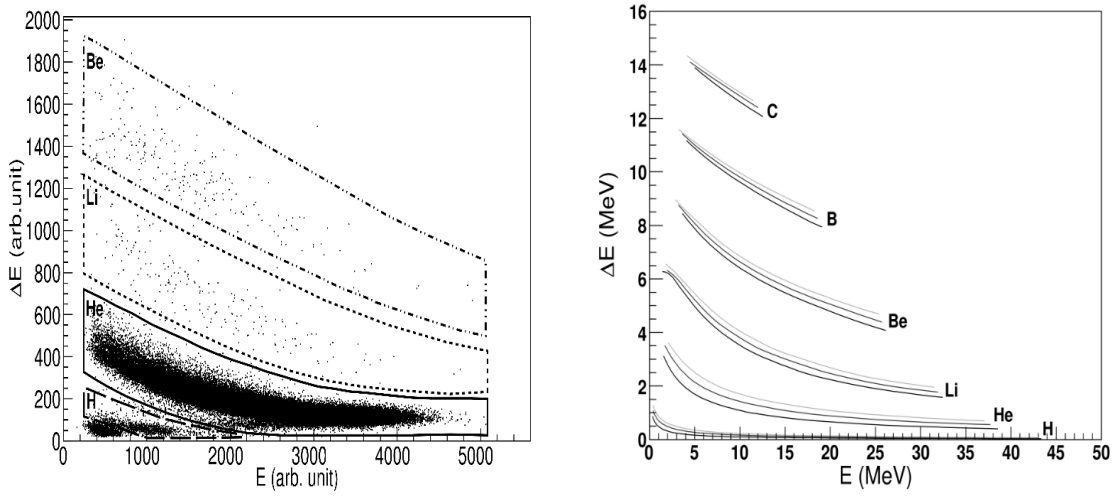

Fig. 2. The experimental (left) and simulated (right) ΔE-E patterns from ternary LCPs. The contour lines define the identification windows used for the analysis. 31 μm thick Al foil was used for protecting the telescopes from being hit by fission fragments and the 6.2 MeV background alpha particles.

3. TERNARY FISSION

A ΔE-E spectrum of LCPs measured (left) and simulated (right) with the telescopes is shown in Fig. 2. Data is created for simulation by SRIM program and simulated spectrum is plotted using ROOT. The contour lines define the identification windows used for the analysis of experimental data (fig.2 (left)). A 31 μm thick Al foil was placed in front of the detectors for stopping the background alpha particles from natural radioactivity of ^{252}Cf (6.2 MeV) in the experiment. The ternary particles from ^{3}H to Be were discriminated as shown in Fig.2 (left). Because of the energy threshold by the ΔE detector, isotopes lighter than ^{3}H are not well resolved in Fig.2 (left). Due to the 31 μm Al foil and 12 μm ΔE detector, the lowest energy (threshold) of α particles which can reach the E detector was about 7.5 MeV. Energy spectra were plotted for identified ternary particles using graphical cut-off method.

The LCP energy spectra obtained with the telescope on the ternary fission modes with He, Li and Be emission are displayed in Fig. 3. All spectra were corrected for energy loss in the absorber foil and the ΔE detector. For the heavier LCP species the accessible range of LCP energy was more seriously limited by the cutoff. This further imposed a strong distortion on the energy spectrum. Heavier LCP particles deposit only part of their energy in the telescopes and were, thus registered at higher energies. Li and Be LCPs emitted in ^{252}Cf ternary fission with kinetic energy over 16.5, 25.5 MeV, respectively, were identified and their relative yields and energy distribution parameters were estimated. A Gaussian fit to the ternary α data points above 12.5 MeV were performed to determine the average energy and sigma, as well as extrapolated counting rates. The results obtained for the various ternary particles are listed in Table. The estimated yields are in agreement with the experimental data from [5].

The highest yield was found for He ternary particles. The yield for Li was less than the yield for Be. It can be explained with stable nucleus.

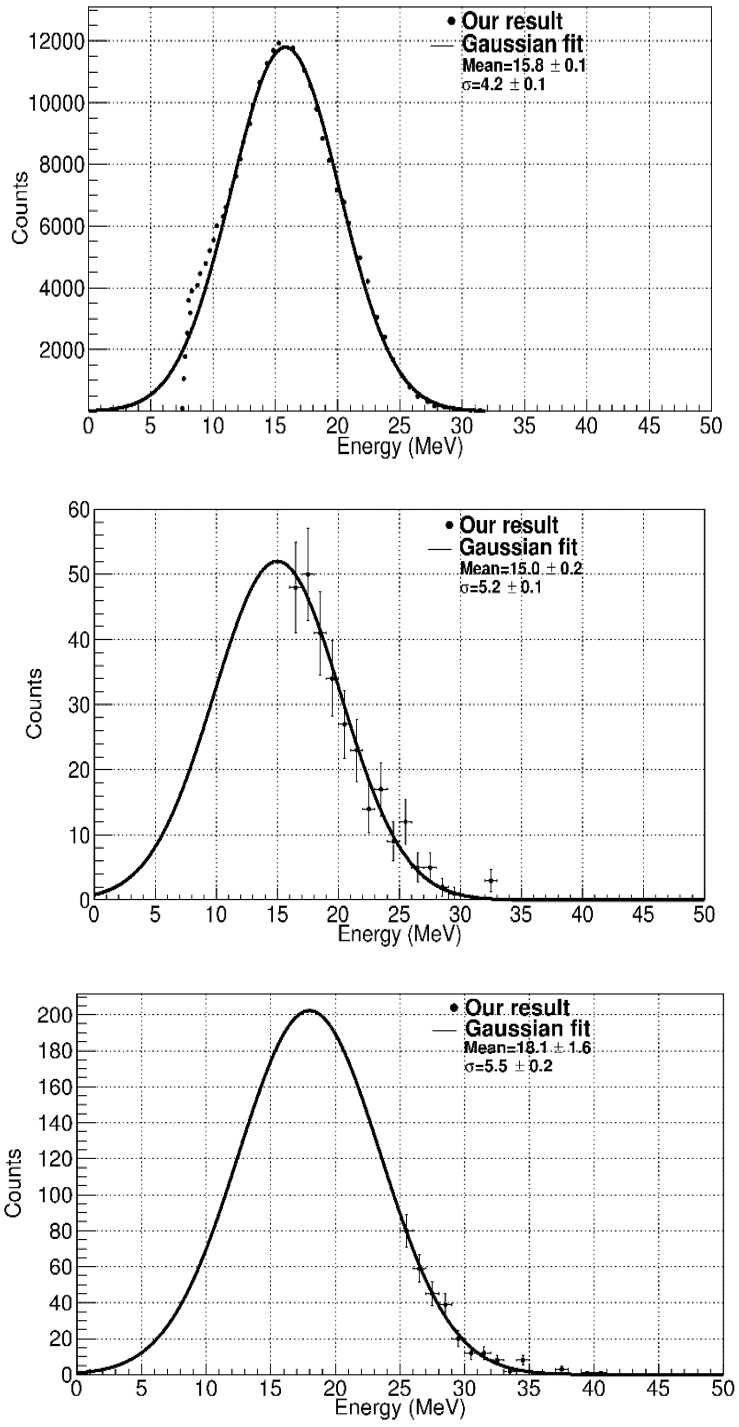

Fig. 3. Energy distribution for the ternary particles He (top), Li (middle) and Be (bottom) emitted in ^{252}Cf(SF), measured with the Al shielding foil. Correction was done for losses on the Al foil and ΔE detector.

Table

Relative emission probabilities of the various ternary particles and the energy distribution for the spontaneous fission of ^{252}Cf

Ternary particles	Events	Threshold energy (MeV)	Energy (MeV)	Sigma (MeV)	Yield per 10^4 α
He	10^5	7.5	15.8(0.1)	4.2(0.1)	10^4
Li	210	16.5	15.3(0.6)	5.2(0.4)	51(11)
Be	214	25.5	18.1(1.6)	5.5(0.2)	224(22)

SUMMARY AND CONCLUSIONS

Ternary particles from spontaneous fission source ^{252}Cf were studied in the experiment. Results obtained are in a good agreement with previous and other work. In addition, ternary particles allowed us to test the response of Timepix detector to different particle species. Compared with other authors' results, the response of Timepix detector to He, Be and Li particles is the same.

---

[1] Proc. Seminar on Fission Pont d'Oye IV, Habay-la-Neuve, Belgium, 2000, p. 59.

[2] *S. Vermote, C. Wagemans, O. Serot, J. Heyse, J. Van Gils, T. Soldner, P. Geltenbort, I. AlMahamid, G. Tian, L. Rao.* Nucl. Phys. A, 837 (2010), p. 176.

[3] *Y. Ronen.* On the light particles in ternary fission. Phys. Scr. 86 (2012) 065203 (6pp).

[4] *Tishchenko V. G., Herbach C.M., Hilscher D., Jahnke U.* Study of ternary and quaternary spontaneous fission of ^{252}Cf with the NESSI detector. Report HMI-B 588, Nov. 2002.

[5] *C. Wagemans* The Nuclear Fission Process (1991).

[6] *G.S. Ahmadov, F.I. Ahmadov et. al.,* ISINN 21 Proceedings (2013).

[7] *X. Llopart et al.,* Nucl. Instr. Meth. Phys. Res. A 581 (2007) 485-494.

[8] *J. Jakubek, et al.*, Nucl. Instr. and Meth. in Phys. Res. A 600 (2009) 651-656.

[9] *V. Kraus, M. Holík, Jakubek et al.,* J. Instrum.6 (2011) C01079.

[10] *D. Turecek, T. Holy, J. Jakubek, S. Pospisil, et al.,* J. Instrum. 6 (2011) C01046.

Received: 24.11.2014

ISSN 1028-8546

2015, Vol. XXI, № 1
Section: En

CONTENTS